UNIVERSITÀ DI PARMA

UNIVERSITA' DEGLI STUDI DI PARMA

DOTTORATO DI RICERCA IN

SCIENZE CHIMICHE

CICLO XXXII

Zwitterionic Coordination Compounds:

Synthesis and Characterization of Co and Pd Metallates

Coordinatore:

Prof. Roberto Corradini

Tutore:

Prof. Daniele Alessandro Cauzzi

Dottorando: Jacopo Andreo

Anni 2016/2019

SUMMARY

Author's Note

This thesis reports most of the work done during my PhD and is divided in three chapters: the first regards palladium coordination compounds, the second cobalt and nickel, and the third focuses on my work at University of California San Diego in the group of prof. Michael J. Sailor on the loading of a molecular thermometer in porous silicon nanoparticles. My stay at UCSD was possible thanks to a RISE project of which prof. Roberto Corradini is a participant. The common feature of these three very diverse chapters is the presence of an organic ligand presenting the unique zwitterionic thioamidyl-phosphonium ($P^{+}C(S)N^{-}R$) moiety.

Before the reader starts this little journey in coordination chemistry a couple of notes for the reader:

- Structures have a common color scheme along the entire thesis to avoid confusion. The key is reported in Figure 0.1.
- A single numeration scheme for organic ligand in the crystallographic structures is employed, also reported in Figure 0.1.

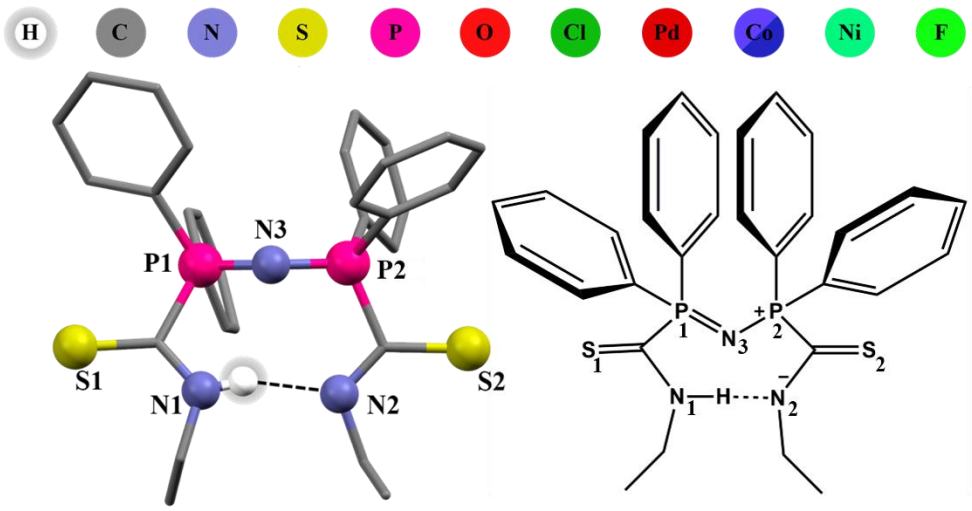

Figure 0.1: Atom color key, scheme and atom numeration for the organic ligand

- We recorded infrared spectra for almost every compound presented in this thesis, to check its purity and confirm the presence of the single desired species by confronting it with the one obtained from the clean crystals. We decided to omit these spectra if they do not add any scientific value to this work, as it has been tuned and filed to be as light and easy to read as possible.

With this out of the way just a quick thanks to my supervisor, prof. Daniele Cauzzi, to prof. Roberto Corradini and to prof. Michael J. Sailor, for the opportunity to spend two wonderful months overseas, and to all my colleagues and friends (with a special note to Dr. Francesca Peccati) that have made all of this possible and kept me (almost) sane during the writing of this thesis.

Experimental Details

INSTRUMENTATION:

- FTIR spectra (4000-400 cm^{-1}) were recorded on a Nicolet Nexus spectrophotometer equipped with a Smart Orbit HATR accessory (diamond crystal).
- ^{1}H NMR (300.13 MHz, TMS) and $^{31}P\{^{1}H\}$ NMR (161.98 MHz, external reference 85% H_3PO_4) spectra were recorder on a Bruker AMX400 spectrometer.
- X-ray diffraction images were recorded on a APEX 2 Bruker diffractometer, the data integrated with CrysAlisPro software from Rigaku and the structures were solved and refined with Olex2 using the ShellX package.

ABBREVIATIONS:

HEtSNS: $EtNHC(S)Ph_2PNPPh_2C(S)NEt$

$EtSNS^-$: $EtNC(S)Ph_2PNPPh_2C(S)NEt^-$

H_2EtSNS^+: $EtNHC(S)Ph_2PNPPh_2C(S)NHEt^+$

HEtSNP: $EtNHC(S)Ph_2PNPPh_2$

HEtSNP: $EtNC(S)Ph_2PNPPh_2$

EtSPO: $EtNC(S)Ph_2PO$

($N(PPh_2S)_2$): tetraphenyldithioimidodiphosphorane

PNP: N,N-Bis(diphenylphosphino)amine

DCM: dichloromethane

DMF: N,N-dimethylformamide

DMSO: dimethylsulfoxide

TFA: trifluoroacetate

HTFA: trifluoroacetic acid

NEt_3: triethylamine

$HNEt_3Cl$: triethylammonium chloride

Introduction

This thesis is focused on the study of zwitterionic organometallates. This family of compounds shows specific features that are consequence of the charge distribution. For this reason, before presenting the compounds that are the object of this research work, the reader will be introduced to the basic concepts underlying zwitterionic compounds. Zwitterionic compounds are systems characterized by a total charge of zero bearing localized formal charges of opposite sign (positive and negative). While this definition, provided by IUPAC is valid in general, particular care must be taken when dealing with metal complexes such as zwitterionic organometallates, containing an organic part and a metal cation.[1] Owing to the multiplicity of formal charges that can be assigned to the metal cation, multiple Lewis structures can be drawn for the same compound, with a variety of charge distribution. If a neutral Lewis structure, i.e. without charge separation, can be drawn for an organometallic complex, then it cannot be defined as a zwitterion, as its definition requires the feature of charge separation. While globally the zwitterionic system is neutral, a word of caution should be spent for the localization of the opposite charges within the molecular architecture. While the charges are generally localized, exceptions occur in the presence of functional groups that are intrinsically delocalized, such as carbonyls. If charge separation is present within a structure, but the net charge is not zero,

the compound takes the name of zwitterion-cation or zwitterion-anion depending on the sign of the total charge, positive or negative respectively.[1]

Charge separation deeply affects the electrostatic properties of zwitterionic compounds compared with non-zwitteronic ones. The main property that is affected is the electric dipole moment p (Eq. 1).

$$p = q \cdot d$$

The electric dipole moment is defined for an ideal system composed of two equal point charges of opposite sign, $+q$ and $-q$ placed at a distance d. The formula given in Eq. 1 indicates that the dipole is directly proportional to both the charge (in our case 1 a.u.) and to the distance between the charges. For this reason, the further apart the localized charges in our zwitterionic system, the larger the dipole moment they originate.

The combined properties of a high dipole moment and globally neutral structure of zwitterions makes them interesting for a number of specific chemical applications, including eluents or stationary phases for chromatography. These combined features are also of interest in the biological field: the requirement of a net charge of zero is stringent in the development of drugs tailored to be able

to cross the Blood-Brain Barrier, which cannot be crossed by charged compounds, and facilitates incorporation into supramolecular architectures. Additionally, charge separation determines to a large extent the optical properties of organic compounds: by encouraging charge transfer transition, zwitterions can be used as chromophores. This is opening new possibilities in perovskites-based solar cells.[2]

Despite this wide range of exciting applications, the main interest of the work presented in this thesis is their complexation properties.

To provide a general reference for understanding zwitterionic complexes, we will now provide a general scheme for how a zwitterionic metal complex can be obtained:

- Reaction between a metal cation and a zwitterionic ligand, an organic molecule that is zwitterionic already in its free state;
- Reaction between a metallic and an organic part of opposite charge, where charges remain separate and the zwitterionic character is the consequence of the rigid association of the two fragments;
- The complexation reaction itself between a metal and a ligand induces charge separation and introduces the zwitterionic character into the compound.

The unique charge distribution of zwitterion compounds is at the origin of the peculiar properties of the family or zwitterionic metallates presented in this work.[3]

A route to the synthesis of ethyl isocyanide is known since the second half of the XIX century which involves the reaction of triethylphosphine with EtNSC, which goes through a zwitterionic intermediate, a thiocarbonyl with a positively charged phosphine substituent on one side, and a negatively charged monosubstituted nitrogen on the other.[4] This example is relevant for our scope because it brings us closer to the description of the family of compounds that are the object of this thesis. Indeed, the main ingredients for our synthesis are heterocumulenes, specifically isothiocyanates, and alkyl-substituted phosphines or phosphinoamines. The displacement of the reaction between isothiocyanates and phosphinoamines towards the reactants or products is regulated by a complex set of parameters, including substituents and environmental effects, such as solvent polarity and viscosity.[5]

In particular, we will focus on the reaction of diphenylphosphineamine (PNP), with ethyl isothiocyanate (Scheme 1). The reaction is initiated by the nucleophilic attack of a P atom of PNP on the carbon atom of the isocyanide (**i**), which breaks the double bond and leads to a thiocarbonyl intermediate with oppositely substituents. This zwitterionic intermediate rearranges transferring a proton from

the neutral N atom adjacent to the positively charged P to the negatively charged N atom from the isothiocyanate, leading to intermediate **A**. This intermediate leaves the second P atom of PNP available for the reaction, that is continued with the same scheme on the other side (**ii**), leading to the second zwitterionic intermediate **1a**, which evolves by eliminating an isocyanate molecule and compound **2**. Alternatively, intermediate A can react with a second molecule of the same type, yielding a highly unstable intermediate that undergoes a

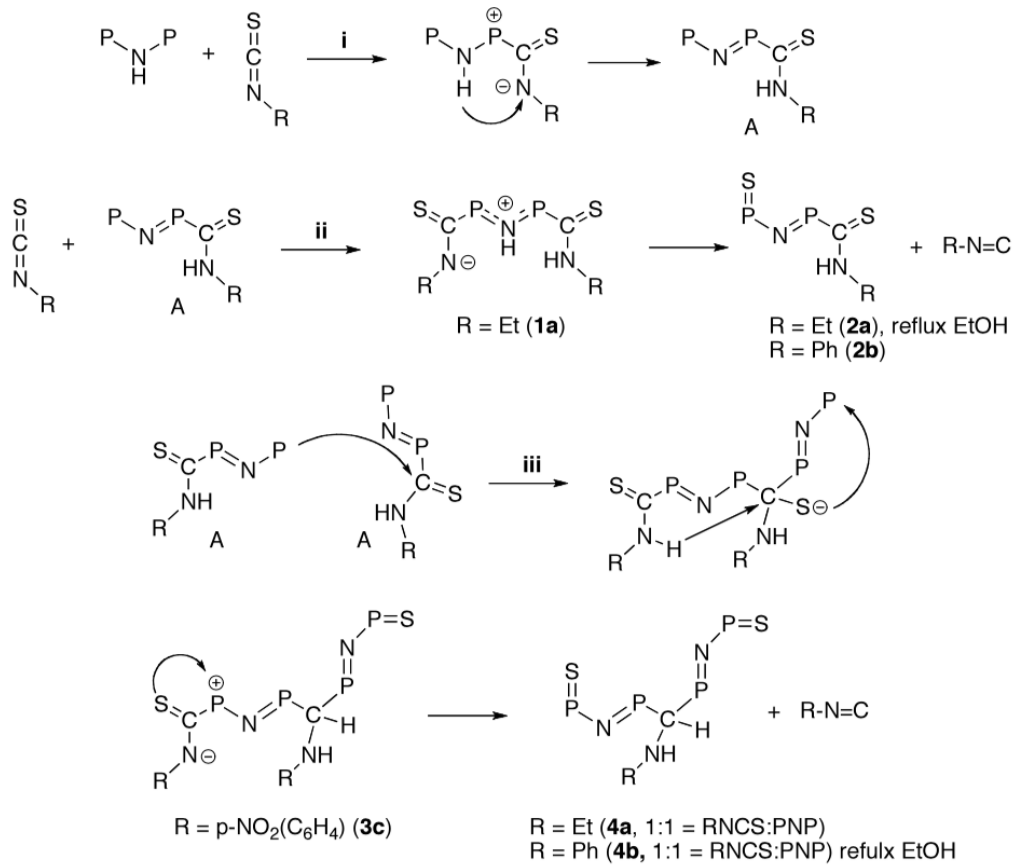

Scheme 0.1: Reactivity of diphenylphosphineamine with ethyl isothiocyanate

rearrangement transferring the sulfur atom to the only remaining free P atom, This, in turn, leads to a redistribution of π electrons that results in a thiocarbonyl group adjacent to an electron deficient phosphorus atom. Transfer of S on P leads to the elimination of an excellent isocyanide leaving group and to the final product 4.[6]

Throughout the research work presented in this thesis, HEtSNS is used as a ligand since it allows the synthesis of compounds with peculiar chemical features. This ligand has been shown to be exceptionally flexible in terms of number of products that can be formed, both through its compatibility with several metal centers and the geometries that can be attained. This flexibility can be explained as follows:

- The ligand can access three protonation states (Scheme 0.2), all of them capable of coordinating metal cations;
- Metal centers can be bound in a mono-, bi- and three-dentate fashion;
- The large charge density on S atoms allows the formation of trimeric adducts, and a large charge density on the metal centers allows the formation of clusters.
- The multiplicity of donating atoms on the metal centers, i.e. the possibility of coordinating metal ions either through S,N,S-κ^3 or N,N,N-κ^3. This work will reveal the first complexes obtained with this ligand featuring the N,N,N-κ^3 coordination, which had previously observed only

with sodium. However, sodium is known to drive the formation of compounds mainly through electrostatics, which does not account for the generation of true coordination complexes. In particular, we will show the formation of NNN Ni and Co complexes.

The coexistence of these features allows for the formation of a wide variety of complexes with a vast selection of metallic centers, and the exceptional electrostatic properties of our ligand make unusual architectures accessible, some of them with peculiar physical properties, leading to a variety of applications.

The most relevant application, published before my Ph.D., is that of the molecular thermometer $[Cu_5(EtSNS)_3](PF_6)_2$. This is a cluster composed of five Cu(I) ions arranged as a trigonal bipyramid. The three ions on the equatorial plane are coordinated by an $EtSNS^-$ lying parallel to the axis of the bipyramid, while the two apical ones are coordinated by the three sulphur atoms of the three ligands. A metal-metal interaction is present between the ions in the apical positions and those in equatorial position. This peculiar organization confers to the cluster its photophysical properties that are the basis of its activity as

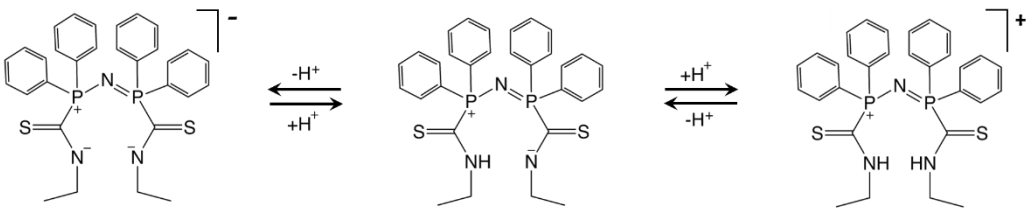

Scheme 0.2: ligand protonation states, from left to right $EtSNS^-$, HEtSNS, H_2EtSNS^+

molecular thermometer. Absorption of a photon at 405 nm leads to a transition from the ground state to a series of seven excited states lying close in energy. All these excited levels but the highest in energy allows radiative deactivation to the ground state. The small energy differences between these states allow their population to follow a Boltzmann distribution. Since the only variable in this distribution is the temperature, the higher its value, the more populated the seventh level. This causes a variation in emission and in the lifetime of the excited states, that directly correlates with the temperature of the system, as the radiative decay decreases when increasing the population of the seventh state. Moreover, experiments in different solvents and quenchers demonstrate that the chemical environment does not affect this phenomenon. This is most likely due to the phenyl moieties present on the three ligands that surround the cluster. As the excited states are centered on orbitals localized on the copper ions forming the cluster core, the effects of solvent polarization cannot reach it.[7]

OBJECTIVES

This thesis has three aims:

1) The extension of our insight into the chemistry of this ligand with elements form the first row of the transition metals, Co and Ni.
2) A deeper understanding of the equilibria of ligand-derived species in solution, with Pd and Co metal centers.

3) The design and development of a nanoparticular composite system with the molecular thermometer which finds application as a cellular thermometer. This last part was carried out during a stay at UCSD in the group of Prof. Sailor.

BIBLIOGRAPHY

[1] a) https://goldbook.iupac.org/terms/view/Z06752 b) R. Chauvin, *Eur. J. Inorg. Chem.* **2000**, *4*, 577-591.

[2] a) A. Pagliara, P. A. Carrupt, G. Caron, P. Gaillard, B. Testa, *Chem. Rev.* **1997**, *97*, 3385-3400. b) V. M. Geskin, C. Lambert, J. L. Bredas, *J. Am. Chem. Soc.* **2003**, *125(50)*, 15651-15658. c) C. Lambert, S. Stadler, G. Bourhill, C. Bräuchle, *Angew. Chem., Int. Ed.* **1996**, *35(6)*, 644-646. d) W. E. Piers, *Chem. Eur. J.* **1998**, *4(1)*, 13-18. e) E. Gerhard, *Chem. Commun.* **2003**, *13*, 1469-1476. f) J. Strauch, G. Erker, G. Kehr, R. Frohlich, *Angew. Chem., Int. Ed.* **2002**, *41*, 2543-2546. g) H. Lee, D. B. Kim, S. H. Kim, H. S. Kim, S. J. Kim, D. K. Choi, Y. S. Kang, J. Won, J. *Angew. Chem., Int. Ed.* **2004**, *43(23)*, 3053-3056. h) Islam, A., Li, J., Pervaiz, M., Lu, Z.-H., Sain, M., Chen, L., Ouyang, X., *Adv. Energy Mater*. **2019**, 9, 1803354.

[3] a)A. Galindo, D. Miguel, J. Perez, *Coord. Chem. Rev.* **1999**, *193*, 643-690. b) H. Schmidbaur, *Angew. Chem., Int. Ed.* **1983**, *22*, 907-927. c) B. Ronig, H. Schulze, I. Pantenburg, L. Wesemann, *Eur. J. Inorg. Chem.* **2005**, *(2)*, 314-320. d) J. C. Thomas, J. C. Peters, *J. Am. Chem. Soc.* **2003**, *125(29)*, 8870-8888.

[4] a) A. W. Hofmann, *Berichte der Deutschen Chemischen Gesellschaft*, **1870**, *3*, 761. b) A. Hantzsch, H.Hibbert, *Chem. Ber*. **1907**, *40*, 1511

[5] a) L. Engel, O. Dahl, *Acta Chem. Scand*. **1974**, *9*, B28. b) K. Akiba, T. Yoneyama, H. Hamada, N. Inamoto, *Bull. Chem. Soc. Japan.*, **1976**, *49(7)*, 1970.

[6] a) D. Cauzzi, M. Delferro, C.Graiff, R. Pattacini, G. Predieri, A. Tiripicchio, *Coordination Chemistry Reviews*, **2010**, 254(5–6), 753-764. b) R. Pattacini, L. Barbieri, A. Stercoli, D. Cauzzi, C. Graiff, M. Lanfranchi, A. Tiripicchio, L. Elviri, *J. Am. Chem. Soc*., **2005**, *128(3)*, 866-876

[7] D. Cauzzi, R. Pattacini, M. Delferro, F. Dini, C. Di Natale, R. Paolesse, S. Bonacchi, M. Montalti, N. Zaccheroni, M. Calvaresi, F. Zerbetto, L. Prodi, Angew. Chem. Int. Ed., 2012, 51, 9662 –9665.

Chapter 1: Palladium

INTRODUCTION

The first metal which we took into account in this thesis is Pd(II). This research line was initiated by Dr. Massimiliano Delferro during his PhD in the group of Prof. Daniele Cauzzi at the University of Parma. His work was devoted to the synthesis of a range of Pd compounds with $EtSNS^-$, obtaining a family of compounds with the general formula $[PdEtSNS]^+X^-$, where X may be either bound to the Pd cation (Cl^-, CN^-), or non-coordinating (PF_6^-). Within this framework, he focused mainly on homo- and hetero cyanide bridged complexes. In the following sections, we will describe the properties of [Pd(EtSNS)Cl] and [Pd(HEtSNS)Cl]Cl, which were firstly synthesized by Delferro.[1] However, despite the fact that these compounds had already been discovered, important questions were still left open, and in particular the presence of non-characterized species at equilibrium [Pd(HEtSNS)Cl]Cl. We unraveled this problem by fully characterizing this new coordination compound at equilibrium in solution and completed this exploration with some density functional theory calculations to confirm the relative stabilities of these species, in collaboration with Dr. Francesca Peccati (Laboratoire de Chimie Théorique, Paris). Very few examples are available in the literature of this kind of equilibria between coordination compounds, none of which concerns palladium compounds; in this sense, the

original work presented in this thesis sheds light on a complex situation and provides a rational interpretation of the behavior of such complex systems, highlighting the importance of factors that are too often overlooked when dealing with complexes of transition metal compounds.[2]

After having achieved a deep understanding of this crucial point, we devoted our attention to three main points: i) the possibility of varying the protonation state of the ligand, ii) the exploration of a new realm of coordination chemistry of the ion Pd(IV) taking advantage of the unique electronic properties conferred by the $EtSNS^-$ ligand, iii) the characterization of degradation products of PdHEtSNS complexes.

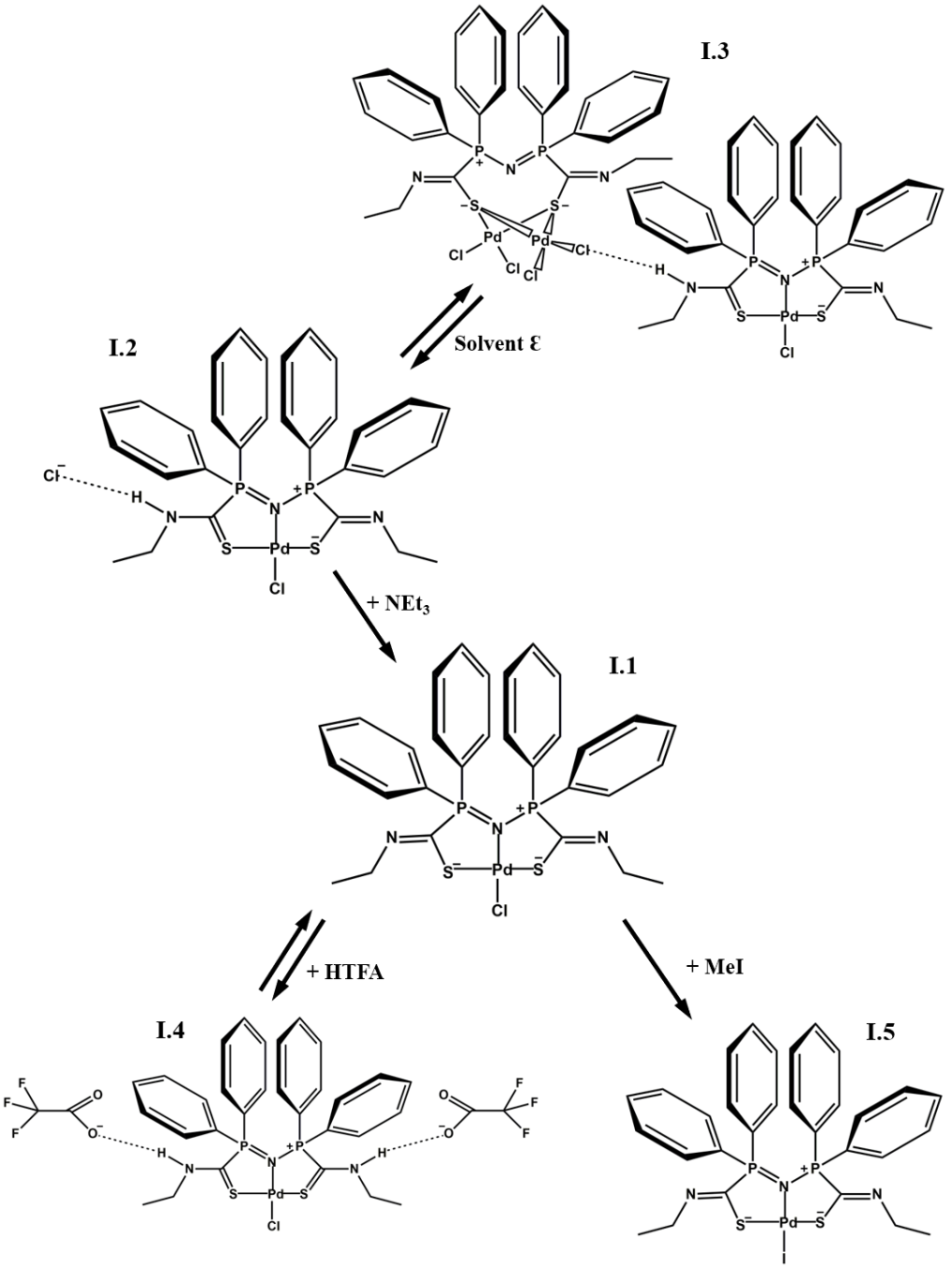

Scheme 1.1

RESULTS AND DISCUSSION

The reaction of HEtSNS with a metallic Pd precursor in the presence of a base leads to the formation of [Pd(EtSNS)Cl] (**I.1**) (Figure 1.1). This compound shows a slightly distorted square planar coordination where the ligand binds in a S,N,S-κ^3 mode, while the fourth position is occupied by a Cl^-. P-N distances between the two phosphor atoms and the central nitrogen are approximately the same, as expected for a delocalized P=N-P^+ moiety. Also, C-S and C-N distances are quite similar. The proton on the thioamidyl group causes the lengthening of the C1-N2 bond; in turn, the C1-S1 distance decreases, resulting in an increased double bond character. A similar behavior was observed for Pd complexes of thioamidic S,N,S pincer ligands.[3]

If the same reaction is carried out without a base, we obtain [Pd(HEtSNS)Cl]Cl (**I.2**) (Figure 1.2), which presents an identical coordination geometry to **I.1**. The

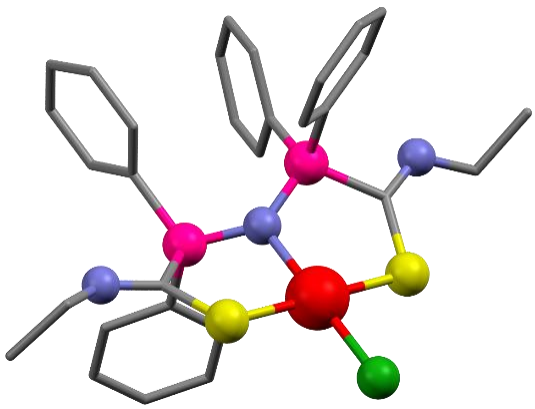

Figure 1.1: [Pd(EtSNS)Cl] (**I.1**)

presence of a hydrogen atom bound to N1 is proven by the formation of a hydrogen bond with the Cl^- out of the coordination sphere, which acts as counterion for the positively charged metal complex. The presence of the proton also leads to the lengthening of the C-N distance on the corresponding thioamidic group, from 1.267 to 1.294 Å and an opposite effect on the C-S bond, that shrink from 1.736 to 1.670 Å. A similar behavior was observed for Pd complexes of thioamidic pincer ligands.

The ^{31}P-NMR spectrum of **I.2** in deuterated chloroform shows three peaks at room temperature, a main one at 36.54, and two lower ones at 12.95 and 5.04 ppm. Our first hypothesis was that the product of the reaction was not unique, and we addressed this issue by selecting by hand, crystal by crystal, the pure XRD-resolved compound. Surprisingly, the ^{31}P-NMR spectrum recorded from these supposedly pure crystals yielded the same number of peaks observed in the

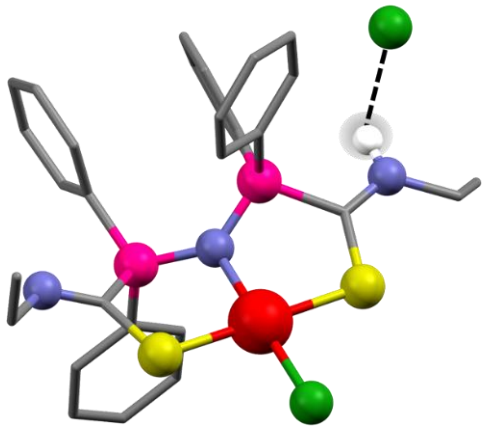

Figure 1.2: [Pd(HEtSNS)Cl]Cl (**I.2**)

previous experiment, indicating that in solution we are in the presence of multiples species in equilibrium with each other. To gain insight, we proceeded to perform temperature-dependent measurements (Figure 1.3); what we observed is that the main peak at 36.5 ppm splits into two below the threshold of 20 °C at 44.9 and 31.2 ppm. The main peak has therefore been assigned to the scrambling of a proton that transfers between the two N atoms (Figure3). At lower temperature, this exchange is slower and we are able to distinguish between the two proton positions. Approaching -60 °C, a fifth peak at 29.6 ppm becomes increasingly well defined.

We also observed that the position and intensity of the other two peaks are Table 1.1) we observe the same three peaks as in chloroform (five at low

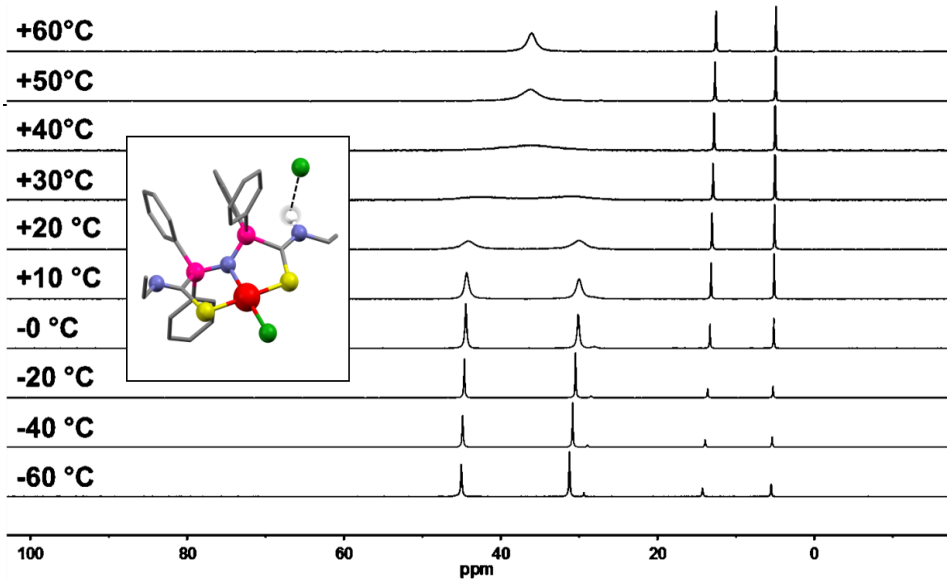

Figure 1.3: ^{31}P NMR spectra of **2** from +60°C to -60°C in $CDCl_3$

temperature), while in methanol the two lower peaks disappear. In toluene and benzene, the lower peaks increase temperature independent. Changing the deuterated solvent used for the NMR, we noticed a further evolution of the pattern of NMR peaks: in most solvents (see Table 1.1) we have the presence of a peak at ~36 ppm, that seems to disappear in toluene. Initially, we believed that the loss of this peak in toluene suggested that we only had the product of the equilibrium in solution, unlike in dichloromethane, where the two species are expected to coexist. While this hypothesis on the position of the equilibrium has been proven correct, the peak at ~36 ppm does not really disappear in toluene, but rather is at coalescence and is not visible as the solubility of the compound limits our resolution. This peculiar behavior observed in the NMR experiments made us focus our attention on these solvents in the search for the other species in

Solvent	**^{31}P peaks (ppm)**			
chloroform	43.49	30.16	12.95	5.04
methanol	39.68		-	-
acetonitrile	37.14		13.39	4.94
acetone	35.8		13.07	4.83
toluene	-		12.68	5.75
benzene	extremely broad		12.56	5.85
dichloromethane	36.54		12.93	5.05
dimethyl sulfoxide	30.6		12.82	-

Table 1.1: ^{31}P NMR peaks of **2** in different solvents

equilibrium, although this was not trivial. Placing hand-picked crystals of compound **I.2** in benzene and toluene, we obtained a saturated solution leading to precipitation of a yellow powder. The only way to crystallize this yellow powder in benzene was to leave the system at -26 °C for a month, while no crystals were obtained from the toluene solution. All other crystallization methods that we tested failed. Only using synchrotron light did we manage to resolve this equilibrium (Reaction 1.1).

3[Pd(HEtSNS)Cl]Cl (**I.2**) → [Pd(HEtSNS)Cl][(PdCl2)2(EtSNS)] (**I.3**)+ H_2EtSNSCl

Reaction 1.1

[Pd(HEtSNS)Cl][(PdCl2)2(EtSNS)] (**I.3**) (Figure 1.4) presents two EtSNS-containing coordination compounds in different protonation states, forming an ion pair. The cationic part is compound **I.2** without the external Cl^-, while the anion is a dinuclear Pd complex with two equivalent $PdCl_2$ moieties bridged by the two sulphurs of a deprotonated $EtSNS^-$, with each of them completing the square planar coordination prescribed by the Pd(II) cation. The Pd-Cl distances are comprised from 2.321 and 2.337 Å, while the Pd-S distances are even more similar, being comprised from 2.282 and 2.293 Å. The two square-planar coordination of the palladium ions are almost co-planar, at an angle of 168°.

After identifying compound **I.3** and thus revealing the stoichiometry of the reaction, we were able to synthesize it pure and with a quantitative yield following Reaction 1.2.

[Pd(EtSNS)Cl] (**I.1**) + [Pd(HEtSNS)Cl]Cl (**I.2**) + $(MeCN)_2PdCl_2$ →

[Pd(HEtSNS)Cl][(PdCl2)2(EtSNS)] (**I.3**)

Reaction 1.2

The reaction involves the deprotonated Pd complex **I.1** with the protonated Pd complex **2** and the Pd precursor (1:1:1 molar ratio).

Owing to this reaction, we were able to crystallize **I.3** in a number of solvents; however, this was not a trivial task. We believe that the main effect of the solvent in this case is how it participates to the three-dimensional structure of the crystals. Since the molecular unit of the crystal is composed of two large charged

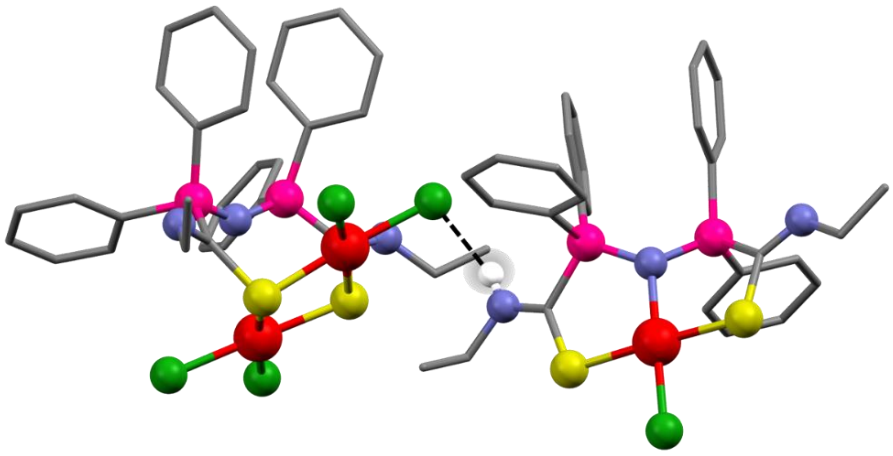

Figure 1.4: $[(PdCl_2)_2(EtSNS)][Pd(HEtSNS)Cl]$ (**I.3**)

molecules linked by a hydrogen bond, solvent molecules play an important role in the three-dimensional architecture of the crystal, affecting crystal stability and leading to fast and easy degradability.

We were able to solve the structure only from dichloromethane (Compound **I.3a**), which still proved challenging. We had to resort to an unorthodox method to mount the crystal on the goniometer head of our instrument. We had to take the crystals with their mother solution, insert them in a 0.2 mm capillary, seal it at both ends and diffract the capillary with the crystal still immersed in the mother solution. This was because in dichloromethane we observe the presence of five partially disordered solvent molecules for each asymmetric unit. The presence of this large abundance of crystallization solvent in the crystal of a molecular complex leads to a fast degradation of the crystalline phase even when immersed in fomblin and at low temperature. This problem was observed for all the solvents that we tested except for benzene, where the crystallization solvent is strongly stabilized by pi-pi interactions, it's molecular weight and the small dimensions of the cyrstals. Even the crystals obtained in benzene are not particularly stable, but these pi-pi interactions allow for a longer crystal lifetime.

A further anomaly of the NMR spectrum is observed in DMSO. One peak appears at 12 ppm, and one at 23. This is no longer an equilibrium, but a reaction. Compound **I.2** is autoprotonated, yielding 50% of product **I.1** and 50%

H2EtSNSCl. [$DMSO_2PdCl_2$] remains in solution. This is a known degradation process, confirmed by X ray diffraction on the crystals of compound **I.1** obtained by slow evaporation.[4]

Since we have a complex situation with multiple species in equilibrium, we could not rely exclusively on the crystallographic structures and we explored the relative stability of candidate structures in solution using computational methods. The formation of compound 3 in apolar solvents is also favored by the reduction of the number of charges in solution: from three units of complex charged +1, with the three associated Cl^- counterions, we obtain a neutral species, a complex with a charge of -1 and a complex with a charge of +1. Simulations were performed with Gaussian09 using the TPSSh density functional, a 6-31+G(d,p) basis set and the PCM solvent model (For further details see ESI).

Density Functional Theory calculations

Density Functional Theory (DFT) calculations have been used to complement our experimental information in two main steps:

- Proposing tentative architectures for the products of the reactions carried out in different solvents;
- Corroborating with reaction free energies the population of Pd at equilibrium in different solvents.

Details about the computational methods and calibration are reported in the Methods section at the end of this Chapter, so that we will briefly mention that the hybrid TPSSh functional has been used in combination with a medium quality double zeta basis set.

The first set of calculations was performed at the beginning of this experimental work, when the focus was to determine the structure of the Pd complex of HEtSNS. In this first stage, two possible architectures for this complex were explored: a first one (CIS), with the two S atoms coordinated in *cis* to the Pd center, and a third one (TRANS) with the ligand chelating the palladium with the two sulphur atoms in *trans* to one another and the central nitrogen in an axial position, and the remaining two *trans* positions coordinated by Cl^- anions. The relative energies of these compounds are reported in the Methods section in gas phase a variety of solvents of varying dielectric constant. Results clearly indicate that **I.2** is by far the most stable architecture, with energy differences that guarantee that the remaining two species do not exist in solution. These additional candidate structures were designed with the following rationale: in both cases two Cl^- anions are directly coordinated to the metal, unlike compound **I.2**, where the second Cl^- remains external. We expected this inclusion of both anions in the metal coordination sphere to stabilize the complex, but this proved wrong. Additionally, the CIS complex was proposed because we knew

from previous research performed by Dr Delferro that the ligand can coordinate palladium in a cis mode, while the TRANS was designed because the ligand is known to coordinate metal cations with similar of larger ionic radius (Cu^+, Ag^+) with a linear coordination geometry.

A further test was performed to assess, beside the preference of the coordination geometry, for the atoms that bind to the metal cation. Indeed, since for Co we observed a NNN coordination, we performed DFT calculations to assess if also Pd could present, even if with lower stability, NNN instead of SNS coordination. Again, the relative stability of the SNS and NNN species has been assessed both in gas phase and in a variety of solvents (see Methods) and it has been determined that Pd shows a strong preference for SNS coordination.

In the second set of calculations, we addressed the relative energies of Pd complexes at equilibrium. In particular, we computed the energy associated to the reaction 1.3:

$$2[Pd(SNS)Cl]Cl + Cl^- + [Pd(HEtSNS)Cl]^+ \rightarrow [(PdCl_2)_2(EtSNS)]^- + [Pd(HEtSNS)Cl]^+ + H_2EtSNSCl$$

Reaction 1.3

While formally this same reaction could have been written with three molecules of [Pd(HEtSNS)Cl]Cl reactants (Reaction 1.1), i.e. three ion pairs as a whole

instead of only two plus the members of the pair considered separately (Cl^- and $[Pd(HEtSNS)Cl]^+$), we chose this approach to maintain the total number of charges in solution on the left-hand side and on the left-hand side of the reaction. In this way, with no net production or reduction of net charges moving from the reactants to the products, we do not expect artificial stabilization effect coming from the use of a varying dielectric constant changing the solvent (see Methods).

We computed the reaction energy in three different solvents of increasing polarity: benzene, dichloromethane and methanol. Each reactant and product has been optimized in the three solvents and frequencies have been computed to ensure that the optimized geometries are minima. This data has then been used to compute the Gibbs free energy of the reaction including entropic and enthalpic contributions through the partition function obtained from the frequency calculation.

The reaction energy is significantly affected by solvent polarity, which effectively shifts the equilibrium from one side of the reaction to the other. In benzene, the least polar of these solvents, we obtain -12.73 kcal/mol, indicating that the reaction is completely shifted towards the products, i. e. we expect a predominance of the dimeric species $[(PdCl_2)_2(EtSNS)]^-$. Conversely, in methanol we obtain 4.92 kcal/mol, which indicates that the equilibrium is fully shifted towards the reactants. Dichloromethane, which has an intermediate

dielectric constant between the two previous solvents, yields a value of 1.68 kcal/mol, which is indicative of a coexistence of reactants and products.

Since population is connected to reaction free energies through the Boltzmann relation, reaction energies must be extremely accurate when predicting population ratios. DFT is by far not the most accurate computational method available but is cost-effective and allows the tackling of such large systems. An error of about 1 kcal/mol is expected to affect these data, but we will still compute the relative population of reactants and products to give the reader a qualitative idea of how these species are distributed. At room temperature, in benzene we expect more than $2 * 10^9$ molecules of product for each molecule of reactant and we can consider it essentially absent. In dichloromethane, approximately five molecules of product are expected each 100 molecules of reactant, while in methanol we expect two every 10000.

Having characterized the multiple species in equilibrium in solution, we can now discuss the reactivity of this compound. This reactivity is direct consequence of self-protonation, as a ligand of a first complex transfers a proton to the ligand of a second complex. The di-protonated complex becomes destabilized and surrenders the palladium ion (with the Cl^- anions) to the deprotonated complex, generating a dimeric structure. From the XRD structure of these product, we were

able to obtain it directly through a different synthetic pathway, confirming their structure and origin.

Although the lower stability of $EtSNS^-$ did not consent us to synthetize the deprotonated palladium complex with HCl, we were able to synthesize the di-protonated palladium with a H_2EtSNS^+ coordinated directly to the metal reacting **1** with a non-coordinating acid, HTFA, obtaining $[Pd(H_2EtSNS)Cl](TFA)_2 \cdot 2HTFA$ (**I.4**) (Figure1.5). This complex is still less stable than the previous ones, as its crystals form a solution containing at least 20% of HTFA; with less acid, only the deprotonated species is obtained. Compound **I.4** again presents a slightly distorted square planar coordination, which differs from that of compound **I.1** for shorter Pd-S (from 2.314 to 2.291 Å) and Pd-Cl bonds (from 2.292 to 2.262 Å) and a longer Pd-N bond (from 2.064 to 2.120 Å). This structure also presents two trifluoroacetate anions acting as counterions to the metal complex, which has a

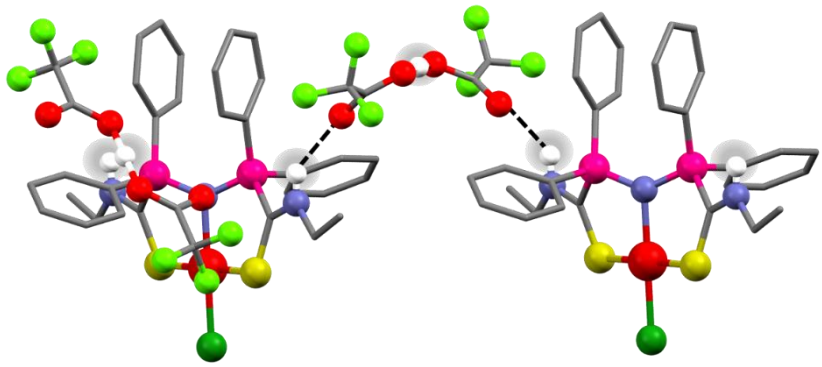

Figure 1.5: $[Pd(H_2EtSNS)Cl](TFA)_2 \cdot 2HTFA$ (**I.4**), two complexes are shown for clarity.

charge of +2. Surprisingly, also two molecules of trifluoroacetic acid are observed in the structure. Each trifluoroacetic acid molecule pair with a trifluoracetate ion, sharing the proton with a short O-O distance (2.419 Å). However, for one of the two TFA-HTFA dimers, this hydrogen bond is not isolated but part of a complex network that extends also to a second and a third equivalent hydrogen bonds between the NH group of the thioamide on adjacent ligand molecules and the free oxygen atoms of trifluoroacetic carboxyls (N-O = 2.836 Å), thus creating a 2D network of hydrogen-bonded complexes and TFA-HTFA dimers.

The peculiar electronic properties of our systems (an unusually high electron density on the metal center) led us to test with a simple reaction the possibility of obtaining a compound of Pd(IV). We reacted compound **I.1** with iodomethane,

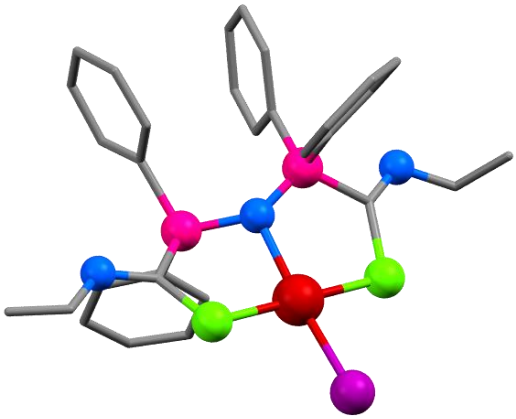

Figure 1.6: [Pd(EtSNS)I] (**I.5**)

expecting oxidative addition to the metal center. This, however, did not lead to the formation of Pd(IV), but rather to the formation of [Pd(EtSNS)I] (**I.5**) (Figure 1.6). Even if compound **I.5** does not present Pd(IV), still the reaction follows our expectations concerning the density on the metal. Indeed, the exchange of halogens on the metal center is a marker of the oxidative addition that has brought I on the metal center, which is then followed by the reductive elimination of MeCl yielding the final product. The ability to undergo this kind of reactions opens the possibility of applying our family of compounds in the field of catalysis, but a deeper exploration is beyond the scope of this thesis.[5]

To conclude, we will discuss the process of ligand degradation. During the research presented in this thesis, we have encountered two degradation of Pd containing complexes. The first was obtained heating compound **I.2** at reflux in toluene, in the search for the species in equilibrium with **I.2**. [Pd(HEtSNP)Cl_2]

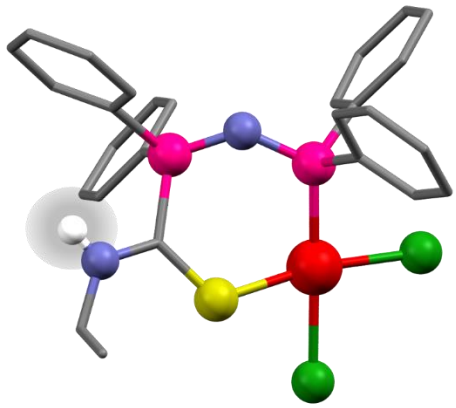

Figure 1.7: [Pd(HEtSNP)Cl_2] (**I.6**)

(**I.6**) (Figure 1.7) presents Pd(II) in a slightly distorted square planar coordination geometry, with two Cl^- in *cis*, a S and a P atom. The coordinating P atom originates from the central PNP system of the ligand, which has lost the isothiocyanate group. Pd-Cl bond distances are 2.409 and 2.326 Å for the one in *trans* with respect to P and S respectively. The Pd-S distance is of 2.282 Å, and the Pd-P of 2.227 Å. This complex is interesting because it represents the first known degradation of HEtSNS coordinated to a metal center where an hydrogen on the nitrogen atom. This protonation makes the net charge of this moiety equal to zero.

The second degraded species is fairly similar to the first, with Pd in square planar coordination. $[Pd(EtSNP)_2]$ (**I.7**) (Figure 1.8) is composed of two equivalent ligands like the one presented in the example above, but deprotonated. Here, Pd-P and Pd-S distances are equivalent due to the symmetry of this compound, and

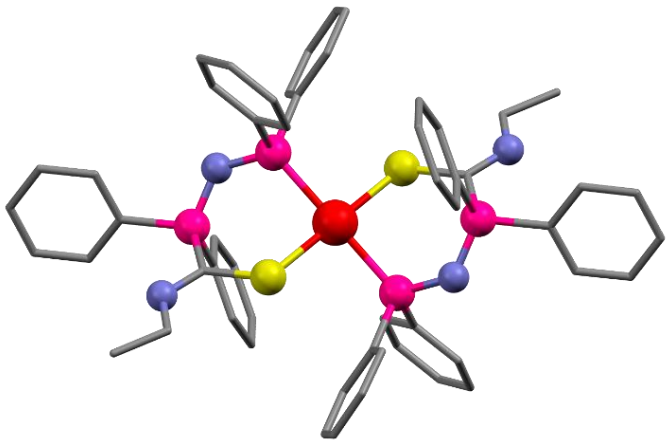

Figure 1.8: $[Pd(EtSNP)_2]$ (**I.7**)

amount to 2.335 and 2.321 Å respectively. It is noteworthy that the trans effect, due to the modification of the ligands in this complex compared with the previous one, severely affects Pd-S and Pd-P bond distances.

CONCLUSIONS

We have explored the complex world of Pd complexation by HEtSNS uncovering a wealth of new structures and exploring the energetic relationship of complex equilibrium in solution. To summarize, we have:

- Achieved a deeper understanding of the chemical properties of this family of compounds through a discussion of their possible catalytic applications and degradation products;

- Unraveled and understood the equilibrium of compound **I.2** in solution;

- Synthesized a new compound with the diprotonated ligand showing that Pd can be coordinated by the ligand in the whole span of its protonation state, which allow us to fine tune the charge on the system.

EXPERIMENTAL SECTION

Preparation of [Pd(EtSNS)Cl] (I.1). Metal precursor [$Pd(CH_3CN)_2Cl_2$] (25.73 mg, 0.1 mmol) and HEtSNS (56.00 g, 0.1 mmol) were dissolved in 5 mL of CH_2Cl_2. 0.075 mL of NEt_3 was added and the reaction mixture was stirred for 30 min. The volatiles were evaporated, and the resulting brown powder was redissolved in 5 ml of CH_2Cl_2. $HNEt_3Cl$ was removed washing three times the reaction mixture with 5ml of water. Evaporation of the solvent afforded complex [Pd(EtSNS)Cl] (**1**) as orange powder. Recrystallization by layering hexane afforded crystals suitable for X-ray diffraction. (Yield 97%) $^{31}P\{^1H\}$ NMR ($CDCl_3$): δ = 25.8 (s) ppm.

Compound	**I.1**
Empirical formula	$PdClS_2P_2N_3C_{30}H_{30}$
Formula weight	700.48
Temperature/K	293(2)
Crystal system	monoclinic
Space group	C2/c
a/Å	13.6943(10)
b/Å	14.8663(15)
c/Å	15.685(2)
α/°	90
β/°	105.878(7)
γ/°	90
Volume/Å^3	3071.3(6)

Z	4
ρ_{calc}g/cm^3	1.515
μ/mm^{-1}	0.957
F(000)	1424
Crystal size/mm^3	0.3 x 0.2 x 0.1
Radiation	MoKα (λ = 0.71073)
2Θ range for data collection/°	4.132 to 55.01
Index ranges	$-17 \leq h \leq 17$, $-19 \leq k \leq 19$, $-20 \leq l \leq 20$
Reflections collected	17996
Independent reflections	3514 [R_{int} = 0.0308, R_{sigma} = 0.0245]
Data/restraints/parameters	3514/2/198
Goodness-of-fit on F^2	1.022
Final R indexes [I>=2σ (I)]	R_1 = 0.0249, wR_2 = 0.0612
Final R indexes [all data]	R_1 = 0.0347, wR_2 = 0.0643

Preparation of [Pd(HEtSNS)Cl]Cl (I.2). Metal precursor [Pd($CH_3CN)_2Cl_2$] (25.73 mg, 0.1 mmol) and HEtSNS (56.00 mg, 0.1 mmol) were dissolved in 25 mL of CH_2Cl_2. The reaction mixture stirred at room temperature for 30 min. Evaporation of the solvent afforded complex [Pd(HEtSNS)Cl]Cl as orange powder. The complex can be recrystallized by layering hexane onto a CH_2Cl_2 solution, affording red crystals of 2·(CH_2Cl_2)1.5. (Yield 94%) $^{31}P\{^1H\}$ NMR (MeOD-d4): δ = 39.4 (s) ppm.

Compound	**I.2** · $2CH_2Cl_2$
Empirical formula	$C_{30}H_{30}ClN_3PdP_2S_2$
Formula weight	864.33
Temperature/K	293
Crystal system	monoclinic
Space group	C2/c
a/Å	13.66(1)
b/Å	14.94(2)
c/Å	5.80(2)
α/°	90
β/°	106.26(7)
γ/°	90
Volume/$Å^3$	3096(2)
Z	4
$\rho_{calc}g/cm^3$	1.503
μ/mm^{-1}	0.949
F(000)	1424
Crystal size/mm^3	0.3 × 0.3 × 0.3
Radiation	MoKα (λ = 0.71073)
2Θ range for data collection/°	3.84 to 56.64
Index ranges	$-17 \leq h \leq 12$, $-21 \leq k \leq 20$, $-20 \leq l \leq 20$
Reflections collected	2714
Independent reflections	8225 [R_{int} = 0.0607, R_{sigma} = 0.0888]
Data/restraints/parameters	8225/9/428
Goodness-of-fit on F^2	0.841
Final R indexes [I>=2σ (I)]	R1 = 0.0509; wR2 = 0.1623

Final R indexes [all data]	R1 = 0.0788; wR2 = 0.193

Preparation of [Pd(HEtSNS)Cl][(PdCl$_2$)$_2$(EtSNS)] (I.3). Metal precursor [Pd(CH$_3$CN)$_2$Cl$_2$] (25.73 mg, 0.1 mmol), Complex **I.1** (70.05 mg, 0.1 mmol) and Complex **I.2** (56.00 mg, 0.1 mmol) were dissolved in 5 mL of CH_2Cl_2. The reaction mixture stirred at room temperature for 1 hour. Evaporation of the solvent afforded complex [Pd(HEtSNS)Cl][(PdCl2)2(EtSNS)] (**I.3**) as red oily powder. Crystals suitable for single crystal X-ray diffraction were obtained layering hexane on a dilute solution of dichloroethane. (Yield 87%) $^{31}P\{^{1}H\}$ NMR ($CDCl_3$): δ = 44.5 (s), 30.0 (s), 5.2 (s) ppm.

Compound	**I.3** · 3C_6H_6
Empirical formula	$C_{78}H_{79}Cl_5N_6P_4Pd_3S_4$
Formula weight	1849.04
Temperature/K	100
Crystal system	monoclinic
Space group	$P2_1/c$
a/Å	13.23630(10)
b/Å	20.9550(2)
c/Å	28.8530(2)
α/°	90
β/°	94.7330(10)

γ/°	90
Volume/Å^3	7975.57(11)
Z	4
ρ_{calc}g/cm^3	1.54
μ/mm^{-1}	1.029
F(000)	3744
Crystal size/mm^3	0.05 × 0.05 × 0.02
Radiation	synchrotron (λ = 0.700)
2Θ range for data collection/°	3.384 to 51.888
Index ranges	-15 ≤ h ≤ 15, -26 ≤ k ≤ 26, -36 ≤ l ≤ 36
Reflections collected	105966
Independent reflections	15670 [R_{int} = 0.0563, R_{sigma} = 0.0278]
Data/restraints/parameters	15670/0/924
Goodness-of-fit on F^2	1.05
Final R indexes [I>=2σ (I)]	R_1 = 0.0383, wR_2 = 0.1119
Final R indexes [all data]	R_1 = 0.0419, wR_2 = 0.1154

Compound	**I.3** · $5CH_2Cl_2$ **(I.3a)**
Empirical formula	$C_{65}H_{72}Cl_{15}N_6P_4Pd_3S_4$
Formula weight	2038.51
Temperature/K	185
Crystal system	triclinic
Space group	P-1
a/Å	12.7351(4)
b/Å	18.0213(5)
c/Å	20.3319(6)
α/°	113.615(3)
β/°	103.858(2)
γ/°	90.260(2)
Volume/$Å^3$	4124.5(2)
Z	2
$\rho_{calc}g/cm^3$	1.641
μ/mm^{-1}	1.354
F(000)	2038
Crystal size/mm^3	0.3 × 0.2 × 0.1
Radiation	MoKα (λ = 0.71073)
2Θ range for data collection/°	3.316 to 52.744
Index ranges	$-15 \leq h \leq 15$, $-22 \leq k \leq 22$, $-24 \leq l \leq 25$
Reflections collected	31571
Independent reflections	16803 [R_{int} = 0.0470, R_{sigma} = 0.0685]
Data/restraints/parameters	16803/157/905
Goodness-of-fit on F^2	1.018
Final R indexes [I>=2σ (I)]	R_1 = 0.0587, wR_2 = 0.1313

Final R indexes [all data]	$R_1 = 0.0892$, $wR_2 = 0.1466$

Preparation of [Pd(H_2EtSNS)Cl](TFA)$_2$ · 2HTFA (I.4). Complex **I.1** (70.05 mg, 0.1 mmol) was dissolved in 2.5 ml of pure TFA. Red crystals, suitable for X-ray difraction, of **I.4** were obtained layering the solution of 1 with a 1:1 mixture of Diethyl Ether and Exane. (Yield of crystallization 73%). $^{31}P\{^1H\}$ NMR (DTFA): $\delta = 49.9$ (s) ppm.

Compound	**I.4**
Empirical formula	$C_{38}H_{34}ClF_{12}N_3O_8P_2PdS_2$
Formula weight	1156.59
Temperature/K	293(2)
Crystal system	monoclinic
Space group	P2/c
a/Å	13.2502(6)
b/Å	16.2638(9)
c/Å	21.3781(11)
α/°	90
β/°	96.362(5)
γ/°	90
Volume/Å^3	4578.6(4)
Z	4
ρ_{calc}g/cm^3	1.678

μ/mm^{-1}	0.727
F(000)	2320
Crystal size/mm^3	0.3 × 0.2 × 0.2
Radiation	MoKα (λ = 0.71073)
2Θ range for data collection/°	3.092 to 52.744
Index ranges	-16 ≤ h ≤ 16, -20 ≤ k ≤ 20, -26 ≤ l ≤ 26
Reflections collected	53227
Independent reflections	9377 [R_{int} = 0.0733, R_{sigma} = 0.0405]
Data/restraints/parameters	9377/0/670
Goodness-of-fit on F^2	1.125
Final R indexes [I>=2σ (I)]	R_1 = 0.1031, wR_2 = 0.2124
Final R indexes [all data]	R_1 = 0.1579, wR_2 = 0.2415

Preparation of [PdEtSNSI] (I.5). Complex **I.1** (70.05 mg, 0.1 mmol) and iodomethane (14.19 mg, 0.1 mmol) or iodobenzene (20.40 mg, 0.1 mmol) were placed in 5 ml of DCM. The mixture was stirred for 1 hour. The volatile was then evaporated and the resulting black powder was redissolved in 5 mL of DCM. The complex was recrystallized by layering hexane on the solution, affording violet-brown crystals of 5. (Yeld 92%).$^{31}P\{^1H\}$ NMR ($CDCl_3$): δ = 24.2 (s) ppm.

Compound	**I.5**
Empirical formula	$C_{30}H_{29}IN_3P_2PdS_2$
Formula weight	790.92
Temperature/K	293(2)
Crystal system	monoclinic

Space group	C2/c
a/Å	13.6331(5)
b/Å	15.3395(4)
c/Å	15.8480(5)
α/°	90
β/°	105.291(4)
γ/°	90
Volume/$Å^3$	3196.88(19)
Z	4
$\rho_{calc}g/cm^3$	1.643
μ/mm^{-1}	1.801
F(000)	1564
Crystal size/mm^3	0.4 × 0.2 × 0.2
Radiation	MoKα (λ = 0.71073)
2Θ range for data collection/°	4.08 to 56.56
Index ranges	$-18 \leq h \leq 18$, $-20 \leq k \leq 20$, $-21 \leq l \leq 21$
Reflections collected	21753
Independent reflections	3968 [R_{int} = 0.0274, R_{sigma} = 0.0150]
Data/restraints/parameters	3968/0/189
Goodness-of-fit on F^2	1.12
Final R indexes [I>=2σ (I)]	R_1 = 0.0413, wR_2 = 0.0956
Final R indexes [all data]	R_1 = 0.0485, wR_2 = 0.1001

Preparation of [Pd(HEtSNP)Cl_2] (I.6). Complex **I.2** (70.43 mg, 0.1 mmol) was dispersed in 20 mL of toluene. The mixture was heated to a reflux until all the solid dissolves. While the solution cools to room temperature small yellow needles start to form and flock in suspension. Very slow evaporation of the mother solution or of a solution of the yellow needles in toluene afforded complex [Pd(HEtSNP)Cl_2] (**I.6**) as yellow thick needles suitable for synchrotron-light X-ray diffraction. (Yield 94%). $^{31}P\{^1H\}$ NMR ($CDCl_3$): δ = 30.4 (s), 19.6 (s) ppm.

Compound	**I.6** · C_7H_9
Empirical formula	$C_{34}H_{34}Cl_2N_2P_2PdS$
Formula weight	741.93
Temperature/K	293(2)
Crystal system	monoclinic
Space group	$P2_1/c$
a/Å	9.3032(2)
b/Å	20.4430(3)
c/Å	17.0719(2)
α/°	90
β/°	97.749(2)
γ/°	90
Volume/$Å^3$	3217.18(9)
Z	4
$\rho_{calc}g/cm^3$	1.532
μ/mm^{-1}	0.9

F(000)	1512
Crystal size/mm^3	0.1 × 0.02 × 0.01
Radiation	synchrotron (λ = 0.700)
2Θ range for data collection/°	3.078 to 55.634
Index ranges	$-12 \leq h \leq 12$, $-27 \leq k \leq 27$, $-22 \leq l \leq 22$
Reflections collected	50395
Independent reflections	7642 [R_{int} = 0.0649, R_{sigma} = 0.0355]
Data/restraints/parameters	7642/0/381
Goodness-of-fit on F^2	1.025
Final R indexes [I>=2σ (I)]	R_1 = 0.0408, wR_2 = 0.1179
Final R indexes [all data]	R_1 = 0.0530, wR_2 = 0.1264

Preparation of [Pd(EtSNP)$_2$] (I.7). Complex **I.1** (70.05 mg, 0.1 mmol) was solubilized in 20 mL of methanol. The mixture was heated to a reflux for 1h. The solvent was then evaporated and the reddish powder obtained dissolved in DCM. The yellow solution is separated from a reddish insoluble powder via centrifugation. Layering hexane on the solution affords suitable f X-ray diffraction yellow crystals. (Yield 81%). $^{31}P\{^1H\}$ NMR ($CDCl_3$): δ = 19.6 (s), 12.4 (s) ppm.

Compound	**I.7**
Empirical formula	$C_{54}H_{50}N_4P_4PdS_2$
Formula weight	1049.38
Temperature/K	293(2)
Crystal system	triclinic

Space group	P-1
a/Å	9.420(2)
b/Å	12.426(3)
c/Å	13.0310(19)
α/°	65.005(3)
β/°	88.085(4)
γ/°	70.141(3)
Volume/$Å^3$	1289.4(5)
Z	1
$\rho_{calc}g/cm^3$	1.351
μ/mm^{-1}	0.605
F(000)	540
Crystal size/mm^3	0.4 × 0.2 × 0.2
Radiation	MoKα (λ = 0.71073)
2Θ range for data collection/°	3.478 to 51.358
Index ranges	$-11 \leq h \leq 11$, $-15 \leq k \leq 15$, $-15 \leq l \leq 1$
Reflections collected	12091
Independent reflections	4817 [R_{int} = 0.0284, R_{sigma} = 0.0287]
Data/restraints/parameters	4817/0/296
Goodness-of-fit on F^2	1.133
Final R indexes [I>=2σ (I)]	R_1 = 0.0363, wR_2 = 0.0891
Final R indexes [all data]	R_1 = 0.0562, wR_2 = 0.1047

COMPUTATIONAL METHODS

1.1 Calibration of the computational method

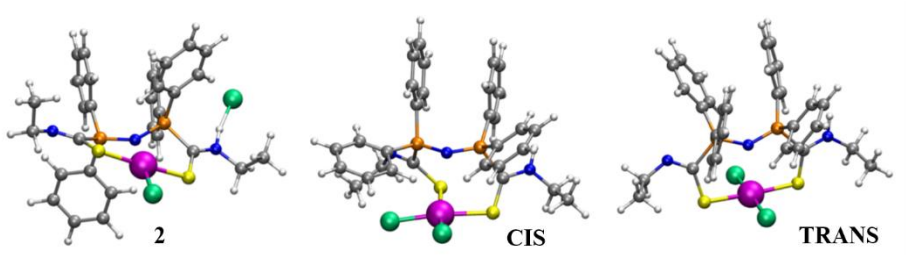

Figure 1.9: The three Pd - EtNHC(S)Ph_2PNPPh_2C(S)NEt complex structures used for calibrating the computation method, dubbed as 2, CIS and TRANS according to the coordination geometry of the Pd center. All structures are closed shell singlet, with a net charge of zero.

The relative potential and Gibbs free energies of the three complexes shown in Figure 1.1 have been used to assess the performance of three DFT functionals: a GGA one, PBE,[6] and two hybrid ones, TPSSh (nonempirical, meta-hybrid, 10% of Hartree-Fock exchange)[7] and M06-2X[8] (empirical, meta-hybrid, 54% of Hartree-Fock exchange). For PBE and TPSSh, Grimme's D3 correction scheme for dispersion has been employed.[9]

The M06-2X functional is parametrized to account for dispersion interactions. Two Pople basis sets, 6-31+G(d,p) and 6-311++G(d,p) were tested in combination with these three functionals.[10,11] Both basis sets include polarization and diffuse functions, fundamental for the description of anions such as Cl-. solvation effects have been introduced with the Polarizable Continuum

Model (PCM) using the integral equation formalism variant (IEFPCM).[12] Frequency calculations have been performed to ensure that all structure are minima of the potential energy surface.

6-31+G(d,p) E gas	**I.2**	TRANS	CIS	G	**I.2**	TRANS	CIS
PBE	0	14.81	15.07	PBE	0	15.7	16.01
TPSSh	0	13.85	13.85	TPSSH	0	15.64	15.17
M06-2X	0	11.78	13.24	M06-2X	0	14.05	15
6-311++G(d,p) E gas	**2**	TRANS	CIS	G	**2**	TRANS	CIS
PBE	0	14.68	14.93	PBE	0	15.62	15.61
TPSSh	0	13.56	13.52	TPSSH	0	15.46	15.49
M06-2X	0	11.04	12.66	M06-2X	0	13.48	14.65
6-31+G(d,p) E MeOH	**2**	TRANS	CIS	G	2	TRANS	CIS
PBE	0	14.65	10.34	PBE	0	14.99	10.63
TPSSh	0	14.74	9.91	TPSSH	0	16.55	11.74
M06-2X	0	13.75	8.42	M06-2X	0	15.32	8.88

Table 1.2: Relative potential (E) and Gibbs free (G) energies in kcal mol-1 for **I.2**, TRANS and CYS in gas phase with the 6-31+G(d,p) basis set, in gas phase with the 6-311++G(d,p) basis set and in methanol with the 6-31+G(d,p) basis set. Methanol has been chosen as representative of polar solvents to assess the effect of a polar medium on the relative stability of the structures. Structure labels refer to Figure 1.1.

The three functionals yield comparable relative energies for the three structures. Interestingly, solvation in MeOH (implicit solvent) stabilizes the CIS structure. This can be attributed to its larger dipole moment (values in Debye: **I.2** = 11, PIR

= 16, CIS = 18). Analysis of the bond distances around the Pd center is presented in Table 1.3.

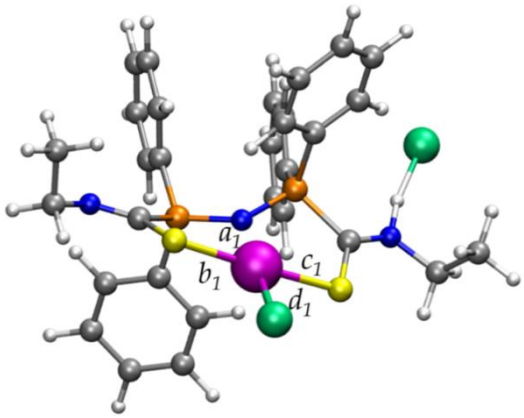

Figure 1.10: **I.2** complex, distances around the Pd centre

Functional	*a1*	*b1*	*c1*	*d1*
I.2 Gas phase, 6-31+G(d,p)				
PBE	2.08	2.34	2.34	2.31
TPSSh	2.07	2.34	2.35	2.3
M06-2X	2.13	2.36	2.42	2.31
I.2 Gas phase, 6-311++G(d,p)				
PBE	2.07	2.34	2.35	2.3
TPSSh	2.08	2.34	2.35	2.3
M06-2X	2.13	2.36	2.42	2.31
I.2 MeOH, 6-31+G(d,p)				
PBE	2.07	2.33	2.35	2.35
TPSSh	2.07	2.33	2.35	2.34
M06-2X	2.12	2.35	2.41	2.36
I.2	2.07	2.29	2.3	2.29

Table 1.3: **I.2** bond distances in Å.

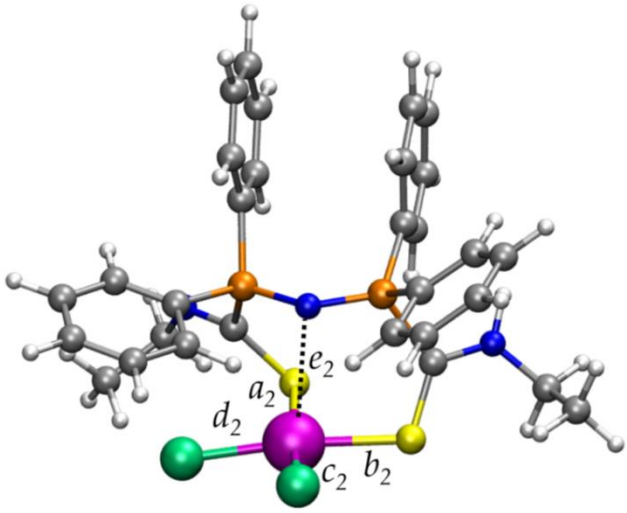

Figure 1.11: CIS complex, distances around the Pd center.

Table 1.4: CIS bond distances in Å

Functional	*a2*	*b2*	*c2*	*d2*	*e2*
CIS Gas phase, 6-31+G(d,p)					
PBE	2.37	2.3	2.38	2.33	3.01
TPSSh	2.37	2.32	2.36	2.32	2.96
M06-2X	2.42	2.41	2.39	2.34	2.94
CIS Gas phase, 6-311++G(d,p)					
PBE	2.37	2.31	2.38	2.34	3.01
TPSSh	2.38	2.32	2.36	2.33	2.96
M06-2X	2.42	2.42	2.39	2.34	2.93
CIS MeOH, 6-31+G(d,p)					
PBE	2.35	2.32	2.41	2.38	3.16
TPSSh	2.35	2.33	2.39	2.38	3.09
M06-2X	2.37	2.39	2.43	2.41	3.09

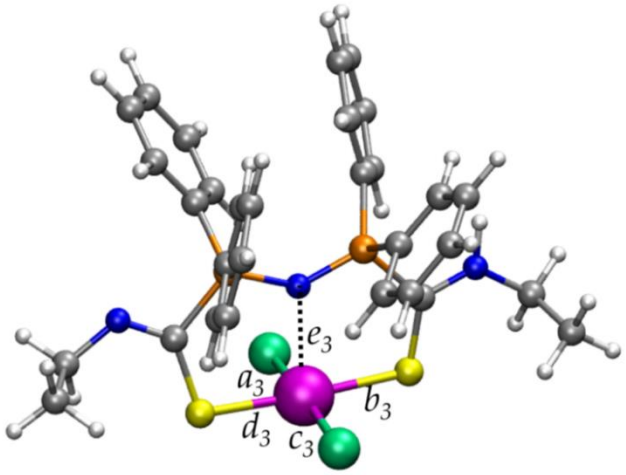

Figure 1.12: TRANS complex, distances around the Pd center.

Table 1.5: TRANS bond distances in Å.

Functional	a3	b3	c3	d3	e3
TRANS Gas phase, 6-31+G(d,p)					
PBE	2.38	2.35	2.38	2.34	2.48
TPSSh	2.37	2.37	2.36	2.34	2.5
M06-2X	2.41	2.49	2.39	2.34	2.6
TRANS Gas phase, 6-311++G(d,p)					
PBE	2.38	2.36	2.38	2.34	2.47
TPSSh	2.37	2.38	2.36	2.34	2.49
M06-2X	2.41	2.5	2.39	2.34	2.59
TRANS MeOH, 6-31+G(d,p)					
PBE	2.39	2.36	2.39	2.33	2.54
TPSSh	2.38	2.37	2.37	2.34	2.53
M06-2X	2.41	2.46	2.42	2.34	2.61

Overall the bond distances around the Pd center do not seem to be much affected by the size of the basis set or the presence of the implicit solvent. M06-2X predicts significantly longer bond distances than PBE and TPSSh. This can be explained in terms of the fraction of HF exchange and the system under study: the similar results obtained with PBE and TPSSh are coherent with the observation that often in transition metal complexes the introduction of the HF exchange only improves slightly the geometry.[13] Comparing M06-2X with TPSSh, it is usually expected that the increasing fraction of HF exchange (10% in TPSSh and 54 % in M06- 2X) accentuates the ionic character of the bond, which can explain the elongation for M06-2X. This point, however, is still debated.[14] For the rest of the calculations presented in this work, we will settle on the TPSSh functional, which performs well for transition metal complexes, taking into account in the Discussion that it sometimes underestimates bond length.

BIBLIOGRAPHY

[1] M. Delferro, Synthesis and Characterization of Zwitterionic Metallates and Molecular Clusters, **2008.**

[2] Y. Kawada, Y. Kataoka, Y. Ura, *Dalton Trans.*, **2013**, 42, 14844-14855

[3] R. A. Begum, D. Powell, K. Bowman–James, *Inorg. Chem*, **2006**, 45 *(3)*, 964-966.

[4] a) G. Sipos, E. E. Drinkel, R. Dorta, *Chem. Soc. Rev.*, **2015**, 44, 3834. b) T. Diao, P. White, I. Guzei, S. S. Stahl, *Inorg. Chem*. **2012**, 51 *(21)*, 11898-11909

[5] P. Sehnal, R. J. K. Taylor, I. J. S. Fairlamb, *Chem. Rev.* **2010,** 110, 824–889

[6] J. P. Perdew, K. Burke, and M.s Ernzerhof. *Phys. Rev. Lett*., **1996**, 77, 3865–3868.

[7] V. N. Staroverov, G. E. Scuseria, J. Tao, and J. P. Perdew. *J. Chem. Phys.*, **2003**, 119 *(23)*, 12129–12137.

[8] Y. Zhao and D. G. Truhlar. *Theor. Chem. Acc.*, **2008**, 120 *(1)*, 215–241.

[9] S. Grimme, J. Antony, S. Ehrlich, and H. Krieg. *J. Chem. Phys.*, **2010**, 132 *(15)*,154104.

[10] R. Ditchfield, W. J. Hehre, and J. A. Pople. *J. Chem. Phys.*, **1071**, 54 *(2)*, 724–728.

[11] A. D. McLean and G. S. Chandler. *J. Chem. Phys*., **1980**, 72 *(10)*, 5639–5648.

[12] S. Miertus, E. Scrocco, and J. Tomasi. *Chem. Phys.*, **1981**, 55 *(1)*, 117–129.

[13] Michael Bühl, Hendrik Kabrede. *J. Chem. Theory Comput*., **2006**, 2 *(5)*, 1282–1290.

[14] E. I. Ioannidis, H. J. Kulik. *J. Chem. Phys.*, **2015**, 143 *(3)*, 034104

Chapter 2: Cobalt and Nickel

INTRODUCTION

Over the last few years, first row transition metals have gained a lot of attention in an effort to replace second and third row transition metals. This is due to their higher abundance, lower cost and lesser environmental impact. However, few examples are available in the literature of complexes of first row transition metals with zwitterionic ligands with architectures such as the ones presented in this thesis. For this this reason, we explored HEtSNS coordination to cobalt and nickel.[1]

Co yielded a large family of compounds in a range of oxidation states, which will be described in the following section. Interestingly, the presence of the first-row transition cation shifts the preferred coordination of the ligand from SNS to NNN, which reflects the different electronic properties of the metal center. This is fascinating because it allows us to explore the coordination of our ligand under a completely new light. This, however, also shows a drawback: by coordinating in a NNN mode, we cannot change the protonation state of the coordinated ligand.

Nickel complexes, on the other hand, proved significantly less stable and yielded a smaller set of new compounds. The study of its reactivity helped, however, to gain insight into the chemical properties of our family of compounds owing to the large number of degradation products observed.

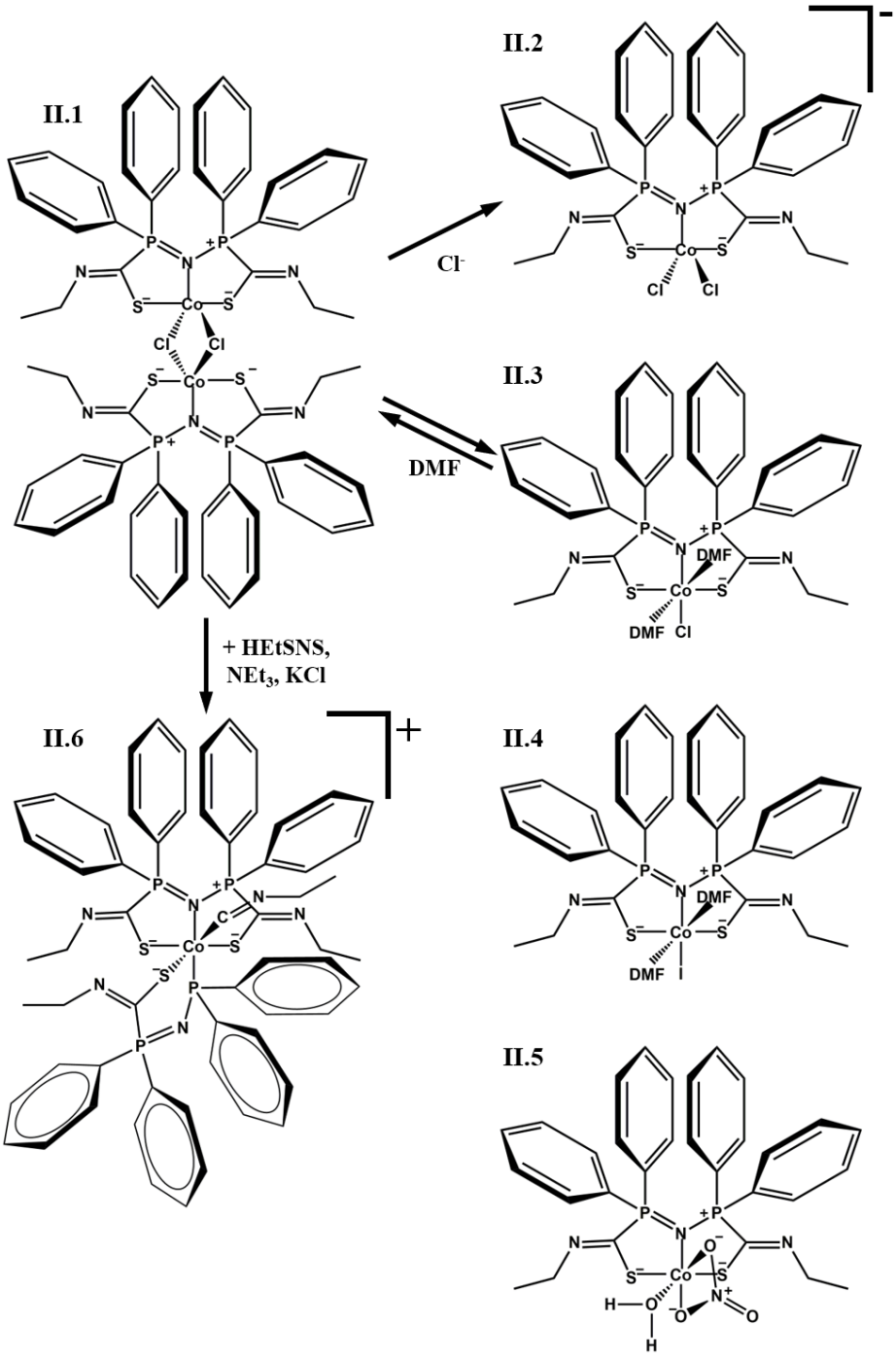

Scheme 2.1

RESULTS AND DISCUSSION

Cobalt is the first transition element for which a N-N-N coordination of our ligand has been observed. The reaction of $[(PPh_3)_2CoCl_2]$ with HEtSNS in the presence of a weak base (NEt_3) in acetone lead to the synthesis of $[Co(EtSNS)Cl]_2$ (**II.1**) (Figure 2.1). Compound **II.1** presents a slightly distorted trigonal bipyramid coordination. One of the axial and both equatorial positions are occupied by the nitrogen atoms of the ligand. The two remaining axial positions are occupied by Cl^- anions, bridging two symmetry equivalent metal centers. Bond distances between Co and the two equatorial nitrogens are almost equivalent (N1-Co = 2.057Å and N2-Co = 2.046Å). The bond distance involving the axial nitrogen is, as expected, slightly longer, 2.203 Å. Cl^- distances from the metal center are Co-eqCl = 2.351 Å and Co-axCl = 2.474 Å. While almost perfectly regular in the axial direction (178.88°), the geometry is distorted in the equatorial direction: the N1-Co-N2 angle is of 136.40°. This leaves the three

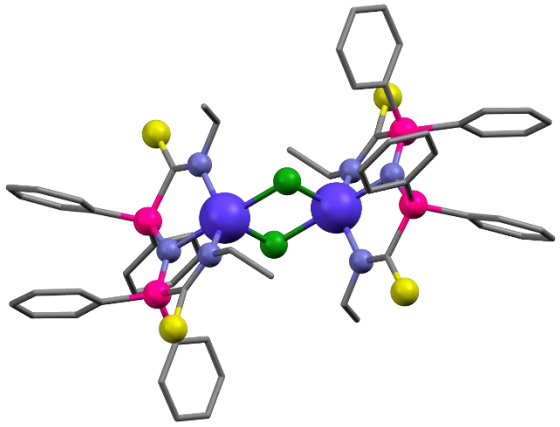

Figure 2.1: $[Co(EtSNS)Cl]_2$ (**II.1**)

nitrogen atoms of the ligand closer to a planar organization than what required by the ideal coordination geometry. A further distortion is observed in the equatorial Cl^- compared to the other two positions, with an N1-Co-Cl angle of 118.72°, and the N2-Co-Cl of 104.13°. This asymmetry is due to the steric hindrance of the ethyl moieties of the two ligands that compose the dimer.

It is noteworthy that the same synthesis in a different solvent, dichloromethane, leads to the formation of $HNEt_3[Co(EtSNS)Cl_2]$ (**II.2a**) (Figure 2.2), that is not a dimer with bridging Cl^-, but rather a monomeric compound. This is due to the incorporation of the triethylammonium chloride salt $HNEt_3Cl$, which is a subproduct of the synthetic process. It is also remarkable how using a different chloride salt, PPh_4Cl, we obtained $PPh_4[Co(EtSNS)Cl_2]$ (**II.2b**), this addition reaction is in equilibrium with **II.1** and how the equilibrium constant varies with the solvent employed. Indeed, while it is necessary to work in excess of salt (1.6) to displace the equilibrium in acetone, lower concentrations are necessary in dichloromethane (1.2). In this reaction, unlike the equilibrium observed for palladium, we do not have a charged-induced driving force (the total number of charges in solution is reduced), but rather we have a neutral species, soluble in this system, that is combined with a soluble charged molecule. We had to test several organic salts due to three reasons:

- The need for a good solubility of the salt in the two solvents;
- The possibility of having systems that can crystallize in these conditions;

- The need for a salt that leads to the formation of non-incommensurate structures in dichloromethane.

The use of triethyl and tetramethylammonium chloride in dichloromethane lead to the formation of two isostructural compounds whose crystallographic structure is incommensurate modulated. An incommensurate modulated crystal structure is a particular case of modulated structure. Normally, a modulated structure (commensurate modulated crystal structure) presents a supercell consistent of a finite number of primitive cells, as the ratio between the modulation vector and the basis structure is a rational number. If the ratio between the modulation vector and the basis structure is irrational, then it is impossible to construct a supercell and the structure is defined as incommensurate, meaning that the periodicity of the crystal and the periodicity of the modulation never repeats in the crystal itself, rending it a particular case of quasi-crystal. An interesting feature of these structures, due to the uncommon character of these structures in molecular

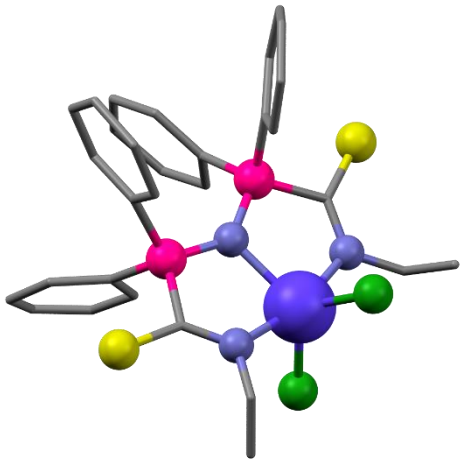

Figure 2.2: $HNEt_3[Co(EtSNS)Cl_2]$ (**II.2a**)

systems, is that the crystals are no longer soluble in the crystallization solvent. We can only speculate on this uncommon behaviour, due to the lack of systems of this kind in the literature, as a systematic study of the properties of these systems is lacking. **II.2** presents an incommensurate structure, in which the metal centre presents a trigonal bipyramid coordination, that involves the three nitrogens of the ligand and the two chlorides. Despite this, the coordination of **II.2** is quite different from the one of compound **II.1**, as the planar positions are not occupied by a chloride and the two nitrogen atom of the thioamidic moiety, but by the central nitrogen of the ligand and the two Cl^-, while the apical positions are occupied by the two thioamidic nitrogens. This change in coordination leads, of course, to a change of the atomic distances, with a shortening of the distances between the Co and the Cl^- (2.289Å), and the Co-N3 (2.120Å from 2.203Å) and a substantial lengthening of the Co-N1 and Co-N2 bond (from 2.057Å and 2.046Å in compound **II.1** to 2.159Å in compound 2). This arrangement leads to less distorted geometry, with the trigonal plane almost undistorted (N3-Co-Cl = 118,89°), and the axial positions (N1-Co-N2 connected by an angle of 166.47°, due to the bite limitations of the ligand.

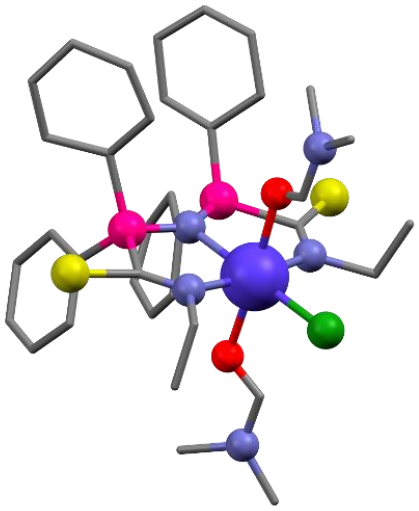

Figure 2.3: [Co(EtSNS)Cl(DMF)$_2$] (**II.3**)

Now, looking at the equilibria in solution, we will describe compound **II.3**. If we add DMF to a solution of **II.1** we establish an equilibrium that leads to the formation of [Co(EtSNS)Cl(DMF)$_2$] (**II.3**) (Figure 2.3). This is indeed an equilibrium, its reversibility is proven by the formation of **II.1** if we solubilize **II.3** in diethyl ether or with a large volume of another solvent to dilute the DMF present and we quench the solution with an antisolvent (such as hexane), thus precipitating the complex. Compound **II.3** has an octahedral coordination, with three equatorial positions occupied by the three nitrogen atoms of the ligand, bound to the metal, the fourth occupied by Cl^- and the two axial ones occupied by DMF molecules. The coordination geometry is only slightly distorted by the trischelated ligand, which presents a bite of 84.25° instead of the ideal 90° due to steric reasons. Unlike the trigonal bipyramid coordination of compounds **II.1** and **II.2**, here Co-N bond distances are more similar to each other, but steric

hindrance prevents them from being perfectly equivalent. Here, distances are N1 - Co= 2.105 Å and N2-Co = 2.182 Å. Also, the Cl-Co distance is intermediate between the ones that have reported previously, with a value of 1.403 Å.

This octahedral compound can be synthesized directly from the reaction in DMF, where it precipitates as a powder, or it can be crystallized both from acetone and dichloromethane adding DMF up to saturation. The important point of these two different crystallizations is that in acetone the process is not affected by the stoichiometric presence of the salt produced in the synthesis, while in dichloromethane this by-product must be eliminated in order to prevent the formation of a mixed system, as the crystals of **II.2a** are not soluble in DCM.

Since these compounds proved stable, we tried to modify their coordination. spheres. This has been done with the following attempts.

- Substitution of chloride or synthesis from Co compounds using heavier halides, Br^- and I^-. Both strategies failed with Br^-, meaning that the desired

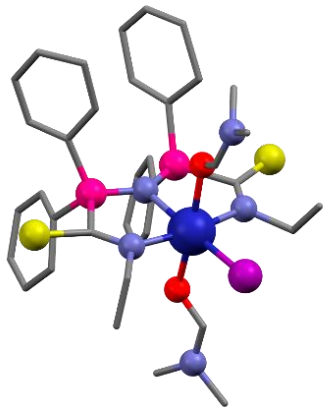

Figure 2.4: Co[(EtSNS)I(DMF)$_2$] (**II.4**)

reactions did not take place, while for iodine only one synthetic strategy was satisfactory, leading to the formation of [Co(EtSNS)I(DMF)$_2$] (**II.4**) (Figure 2.4)**.** This compound is isostructural to compound **II.3**, with Cl^- being replaced by I^-. This leads to a distortion compared with compound **II.3**, with a longer halogen-Co bond, 2.518 vs 2.403 Å. Also the central N of the ligand-Co bond increases (here N3, N2 in compound **II.3**), moving from 2.182 to 2.271 Å. This compound however, unlike the chlorine one, proved labile if solubilized in non-coordinating solvents and not completely stable even in the same solution. This may be due to a phenomenon reported in the literature, i.e. that the presence of iodides prevents the formation of stable dimers or pentacoordinated compounds with two coordinating iodides due to steric hindrance.

- Substitution of the DFM molecules with other ligands. Triphenylphosphine, present in the synthetic precursor of **II:1**, is not incorporated in the final product, while the DMF, used as a solvent, is present in the coordination sphere of **II.3**. This suggests a strong influence of steric hindrance on the possibilities of incorporation of neutral ligands in the coordination sphere of the cobalt. A stronger ligand with a steric hindrance comparable to DMF is N,N'-dimethylthiourea. However, if we add this specie to a solution of compound **II.1**, we do not observe the formation of an octahedral compound analogue to **II.3**. Instead we observe a ligand exchange reaction whereby both Cl^- ions present in the dimer are transferred to a single cobalt center, which coordination sphere is

completed by two N,N'-dimethylthioureas. The stoichiometry of the reaction suggest the formation of an unstable cobalt complex, composed of two $EtSNS^-$ coordinated to the same Co(II) center. This complex, if formed, is not stable, and we obtain, instead, the degradation of $EtSNS^-$ to tetraphenyldithioimidodiphosphorane ($N(PPh_2S)_2$) and the formation of the complex $[Co(N(PPh_2S)_2)_2]$, already reported in literature.[2]

- The third strategy involved chloride substitution with non-coordinating anions. In both the absence and presence of neutral ligands we observed degradation of the ligand itself. Using a Co precursor ($Co(NO_3)_2$), we managed to obtain only one compound, $[Co(EtSNS)(NO_3)(H_2O)]\cdot 2DMF$ (**II.5**) (Figure 2.5).

Compound **II.5** presents a highly distorted octahedral coordination. This is mainly due to the fact that two coordination sites are occupied by the nitrate ion (bidentate). The remaining two positions on the same plane are skewed and occupied by the central N of the ligand and a water molecule. The angle between

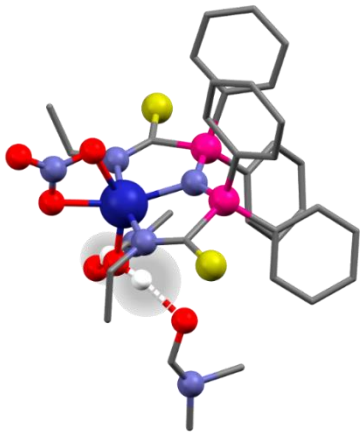

Figure 2.5: $[Co(EtSNS)(NO_3)(H_2O)]\cdot 2DMF$ (**II.5**)

these two ligands is of 109.42°. Bond distances between the metal center and the three N atoms of $EtSNS^-$ are likewise perturbed by the change in coordinating ion, becoming shorter than those of compound **II.3**: 2.085 Å for N1-Co and 2.083 Å for N2-Co, the external ones, and 2.122 Å for the central one (N3). The coordinated water molecules form two hydrogen bonds with two DMF molecules, one of which is disordered in two distinct positions.

However, like in the case of iodide, this compound was stable only in DMF, and not in non-coordinating solvents.

- The third strategy involved reacting compound **II.1** with a metal complex of $EtSNS^-$ and a metal center with chloride scavenging properties, in order to achieve the elusive compound with two $EtSNS^-$ coordinated to a single cobalt ion. We tested [AgEtSNS], [TlEtSNS] and [NaEtSNS], but we observed either lack of reactivity (Ag) or the formation of degradation products. We had more success with a different approach: reacting **II.**1 with HEtSNS, a base and a chloride scavenging salt (either KPF_6 or $TlPF_6$). With this synthetic pathway we obtained [Co(EtSNS)(EtSNP)(EtNC)]PF_6 (**II.6**) (Figure 2.6).

This octahedral compound presents a pristine $EtSNS^-$ compound and a partially degraded one, where both degradation fragments are coordinated to the Co(III). The two fragments have the following architectures: one of the C-P bonds breaks. These bonds result from the reaction of ethilisothiocyanide and PNP. Counting the atoms in the two fragments, it can be noted that the sulphur of isothiocyanate

is no longer present in the structure. In the reaction carried on with $TlPF_6$ we observe the formation of Tl_2S as a black mirror on the vial walls. The oxidation of the cobalt center, from 2+ to 3+, is balanced by the reduction of the phosphor bonded to it, that goes from 4+ to 3+.

This leaves coordinated to Co an ethyl iso-nitrile. This is unexpected because iso-nitrile is itself an unusual ligand, and it is normally found coordinated to metal centers with oxidation number zero, while in this case we have +3. To the best of our knowledge, this is the first case ever reported of iso-nitrile bound to Co(III).

We have scrutinized the possibility of an isomerization, i.e. the fact that the ligand is indeed a nitrile and not an iso-nitrile, but three evidences suggest that indeed we have synthesized the first Co complex with iso-nitrile. The three pieces of evidence are the following:

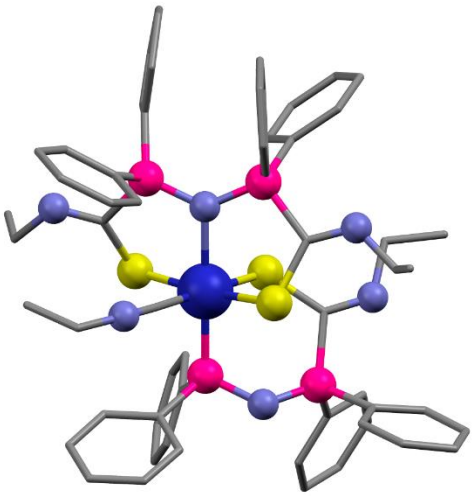

Figure 2.6: [Co(EtSNS)(EtSNP)(EtNC)]PF_6 (**II.6**)

- X-ray diffraction data do not generally allow for a straightforward assignment of C or N atoms on the nitrile group; however, we have diffraction data obtained with synchrotron light, i.e. of high quality. The structural resolution with a nitrile instead of an iso-nitrile worsens the R1 value by a non-negligible 0.25%, suggesting that the ligand is indeed coordinated through the carbon atom;
- To isomerize, the isonitrile has to leave the coordination sphere of the metal; Based on this consideration, we designed an experiment to confirm that the ligand does not detach from the metal. This has been done by simply adding some drops of acetonitrile to the reaction mixture; the rationale between this addition is that propylnitrile (the product of isomerization of our iso-nitrile) and acetonitrile are similar. For this reason, since we are now working in excess of acetonitrile, if the iso-nitrile was labile, we would expect some incorporation of acetonitrile in the coordination sphere of the metal. Since this is not observed, we can conclude that iso-nitrile is a kinetically stable ligand;

  Even if ^{13}C spectra are the common way to proceed when having to distinguish between the two coordination situation, interpretation of results is not trivial as no reference is available for an isonitrile on Co(III). In literature we have found that coordinated nitrile moieties on Co (III) have ^{13}C a chemical shift of around 150 ppm, that is not present in

compound 6 spectrum, while isonitriles have lower shifts compared to nitriles. In our compound ^{13}C spectrum there are various peaks between 135 and 120 ppm, one of which could be assigned to the isonitrile moiety. However, were not able to discern it from the 48 carbons of the phenyl groups.[3]

It is noteworthy that the coordination of the $EtSNS^-$ on Co(III) is no longer NNN, but SNS. Overall, three S atoms are present, two from the pristine $EtSNS^-$ ligand (S1 and S2) and one from the partially degraded one (S3). Surprisingly, no significant difference in the bond distances is observed between the two types of S atoms.: Co-S1 = 2.284 Å, Co-S2 = 2.268 Å, Co-S3 = 2.265 Å. The distance between the central N of the $EtSNS^-$ ligand, N3, and Co is of 2.188 Å. This N3-Co distance is very similar to that of compound **1**, which was 2.196 Å. The Co-P distance is of 2.212 Å.

We will now draw some consideration based on the electronic properties of these compounds. According to classical coordination chemistry, the softer Co(II) should prefer S over N. while the harder Co(III) center should prefer N. Our hypothesis to explain this bizarre behaviour is due to the fact that S is able to donate a stronger amount of electron density on the metal center, thus stabilizing the higher positive charge, in a more electrostatic framework for the description of the binding properties. At this point, given this redox reaction on the metal

centre, we tested several routes to obtain other Co-EtSNS compounds with a variety of oxidation states. All these attempts failed. They will be quickly described in the following paragraph.

The strategy applied to both Co(I) and Co(III) has been twofold. First, we tried to react the ligand with both Co(I) and Co(III) precursors, but in the case of Co(I) this lead to a dismutation of Co, leading to the formation of compound I and Co(0), while we could not react directly Co(III) with our ligand. The second strategy involved applying reducing or oxidizing agents directly on our compounds, but in both cases this leads inevitably to ligand degradation.

Only in one reaction we were able to grow crystals suitable for X-ray diffraction in order to gain insight on the reaction pathway. Compound [Co(EtSNS)(EtSPO)] (**II.7**) (Figure 2.7) is a reaction intermediate in an attempt to reduce the cobalt (II) to Co (I), sensitive to air and moisture. For this reason the quality of the data

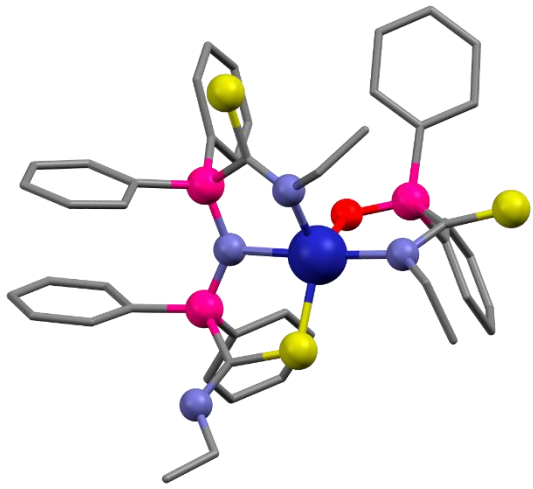

Figure 2.7: [Co(EtSNS)(EtSPO)] (**II.7**)

is much less than ideal, as there was no practical way to diffract the crystals without a strong loss of crystallinity. We will not comment the bond lengths or the angles, as we do not retain the data sufficiently accurate to depict correctly these parameters, but we will briefly comment the general atomic disposition, as it is particularly unusual.

The two main features of this structure are:

- A not degraded $EtSNS^-$ is present, coordinating the metal center through two nitrogen and one Sulphur atom. This feature has been observed only in this crystal;
- A second ligand is present, a partially degraded molecule obtained through a reaction path that has not been observed for other cations. This is characterized by, instead of a first cleavage of the link between the phosphinamine fragment and the isothiocyanate, the cleavage of the phsophinamine with insertion of an oxygen atom on the phosphorus. This oxygen coordinates the metal center.

After obtaining the Co compounds presented in the previous sections of this chapter, and given the good number of structures that has been obtained, we decided to apply the same synthetic strategies to achieve complexes of nickel (Ni(II)). However, the lack of stability of the compounds obtained with HEtSNS and $NiCl_2$ prevented the obtention of the full set of compounds observed for Co,

but still provided useful insight into the degradation mechanisms of this family of complexes. Indeed, the only family of Ni compound which we managed to synthesize with a non-degraded $EtSN^-$ molecule was prepared starting from $Ni(NO_3)_2$ or $Ni(Ac)_2$ in DMF in the presence of a base, with a similar methodology employed for compound **II.4** of Co. As this previous one, it is only stable in DMF.

Compound $[Ni(EtSNS)(NO_3)(H_2O)]\cdot 2DMF$ (**II.8a**) (Figure 2.8a) is isostructural with compound **5**. We obtained crystals of compound $[Ni(EtSNS)(NO_3)(DMF)]$ (**II.8b**) (Figure 2.8b), which has a DMF instead of a water molecule in the coordination sphere of the metal and retain the same coordination sphere for the other five positions. We also obtained compound $[Ni(EtSNS)(CH_3COO)(DMF)]$ (**II.8c**) (Figure 2.8c), which only differs from compound **II.8a** in the presence of an acetate instead of a nitrate, being isostructural for all the rest. It is noteworthy that cobalt acetate as a precursor did not lead to the formation of any complex.

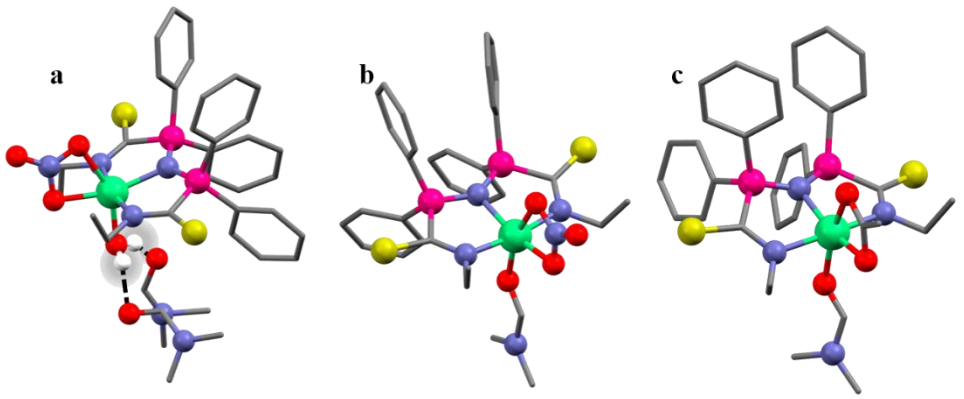

Figure 2.8: a: $[Ni(EtSNS)(NO_3)(H2O)]\cdot 2DMF$ (**II.8a**), b: $[Ni(EtSNS)(NO_3)(DMF)]$ (**II.8b**), c: $[Ni(EtSNS)(CH_3COO)(DMF)]$ (**II.8c**)

It has however been possible to characterize two compounds resulting from ligand degradation obtained both from **8** and from direct reaction of Ni chloride and HEtSNS. Compound [Ni(EtSNP)$_2$] **II.9** presents a degradation product of the ligand resulting from the loss of one of the two isothiocyanides and is essentially isostructural with Pd compound **I.7**, with some difference in the S-M and P-M bond distances: S-Ni = 2.225 Å vs S-Pd =2.321 Å and P-Ni = 2.261 Å vs P-Pd = 2.335 Å. This is in line with the difference of ionic radius between the two cations.

In palladium compounds, we have never observed further ligand degradation leading to the formation of [Ni(N(PPh$_2$S)$_2$)$_2$], already known in the literature, where HEtSNS is completely degraded into bis-diphenyltiophosphonamine.[4]

CONCLUSIONS

We have analyzed Co coordination by $EtSNS^-$ discovering a number of new structures and have in general explored coordination of first row transition metals.

Summarizing we have:

- Discovered that $EtSNS^-$ preferentially binds to Co in an NNN mode, unlike heavier metals;
- Discovered an incommensurate structure (work in progress) with peculiar properties;
- Proven that for Co and Ni, changing the counterion (which can be coordinating or not) has a more marked effect on compounds stability compared with heavier metals.

EXPERIMENTAL SECTION

Preparation of [Co(EtSNS)Cl]$_2$ (II.1). Metal precursor [Co(PPh$_3$)$_2$Cl$_2$] (65.44 mg, 0.1 mmol) and HEtSNS (56.00 g, 0.1 mmol) were dissolved in 5 mL of CH_2Cl_2. 0.075 mL of NEt_3 were added and the reaction mixture was stirred for 1 hour. The volatiles were evaporated, and the resulting green powder was subilized in 5 ml of acetone. $HNEt_3Cl$ was centrifuged and removed. Recrystallization by layering hexane onto the solution afforded dark green crystals of **1**. (Yield 89%)

Compound	**II.1**
Empirical formula	$C_{30}H_{30}ClCoN_3P_2S_2$
Formula weight	653.01
Temperature/K	293(2)
Crystal system	monoclinic
Space group	$P2_1/n$
a/Å	9.0864(2)
b/Å	15.6561(4)
c/Å	20.6580(4)
α/°	90
β/°	82.589(2)
γ/°	90
Volume/Å^3	2914.21(11)
Z	4
ρ_{calc}g/cm^3	1.488
μ/mm^{-1}	0.947
F(000)	1348
Crystal size/mm^3	0.07 × 0.05 × 0.05
Radiation	synchrotron (λ = 0.6199)
2Θ range for data collection/°	3.468 to 48.82
Index ranges	$-12 \leq h \leq 12$, $-20 \leq k \leq 19$, $-27 \leq l \leq 27$
Reflections collected	46072

Independent reflections	7033 [R_{int} = 0.0631, R_{sigma} = 0.0333]
Data/restraints/parameters	7033/0/354
Goodness-of-fit on F^2	1.076
Final R indexes [I>=2σ (I)]	R_1 = 0.0449, wR_2 = 0.1267
Final R indexes [all data]	R_1 = 0.0480, wR_2 = 0.1289

Preparation of X[Co(EtSNS)Cl_2] [X = $HNEt_3$ (II.2a), PPh_4 (II.2b)]. 0.1 mmol of **1** (130.61 mg) were dissolved in 5 mL of CH_2Cl_2. 0.2 mmol of $HNEt_3Cl$ (27.52 mg) or PPh_4Cl (74.96 mg) were added to obtain compound **II.2a** or **II.2b** respectively. Suitable crystals for X-ray diffraction were obtained just waiting the grouth of violet crystals from the green solution in case of $HNEt_3Cl$, while for PPh_4Cl the violet solution was layered with hexane. (Yield 94%)

Compound	**II.2a**
Empirical formula	$C_{36}Cl_2CoN_4P_2S_2$
Formula weight	2968.65
Temperature/K	293(2)
Crystal system	monoclinic
Space group	$P2_1/n$
a/Å	17.89550(10)
b/Å	42.9938(4)
c/Å	21.1745(2)
α/°	90
β/°	97.6340(10)
γ/°	90
Volume/$Å^3$	16147.2(2)
Z	16
$\rho_{calc}g/cm^3$	1.221

μ/mm^{-1}	0.738
F(000)	5855
Crystal size/mm^3	0.2 × 0.15 × 0.15
Radiation	synchrotron (λ = 0.700)
2Θ range for data collection/°	2.932 to 51.888
Index ranges	-22 ≤ h ≤ 22, -53 ≤ k ≤ 53, -26 ≤ l ≤ 26
Reflections collected	215357
Independent reflections	33036 [R_{int} = 0.0510, R_{sigma} = 0.0296]
Data/restraints/parameters	33036/0/1744
Goodness-of-fit on F^2	4.324
Final R indexes [I>=2σ (I)]	R_1 = 0.1563, wR_2 = 0.4823
Final R indexes [all data]	R_1 = 0.1659, wR_2 = 0.4987

Compound	**II.2b** · CH2Cl2
0.1 × 0.07 × C30:D480.07	$C_{55}H_{52}Cl_4CoN_3P_3S_2$
Formula weight	1112.75
Temperature/K	293(2)
Crystal system	orthorhombic
Space group	$Pna2_1$
a/Å	30.921(2)
b/Å	17.6987(14)
c/Å	9.6077(7)
α/°	90
β/°	90
γ/°	90
Volume/$Å^3$	5258.0(7)
Z	4
$\rho_{calc}g/cm^3$	1.406
μ/mm^{-1}	0.741
F(000)	2300
Crystal size/mm^3	0.1 × 0.07 × 0.07
Radiation	MoKα (λ = 0.71073)
2Θ range for data collection/°	3.498 to 46.51

Index ranges	$-34 \leq h \leq 34, -19 \leq k \leq 19, -10 \leq l \leq 10$
Reflections collected	47121
Data/restraints/parameters	7554/1/615
Goodness-of-fit on F^2	1.032
Final R indexes [I>=2σ (I)]	$R_1 = 0.0874$, $wR_2 = 0.1433$
Final R indexes [all data]	$R_1 = 0.1639$, $wR_2 = 0.1777$

Preparation of [Co(EtSNS)Cl(DMF)$_2$] (II.3). 0.1 mmol of metal precursor $CoCl_2$ (25.73 mg) were dissolved with an equimolar amount of HEtSNS (56.00 mg) in DMF. 0.075 mL of NEt_3 were added and the reaction was stirred for 1 hour. Almost immediately a fine gray powder started to precipitate from the green solution. After one hour the mixture was centrifuged and washed three times with fresh DMF. Crystals suitable for X-ray diffraction were obtained redissolving the gray powder in acetone, adding DMF to the solution until it started to cloud. The mixture was then centrifuged and the clear solution stratified with a 1:2 mixture of hexane and diethyl ether. (Yield 94%)

Compound	**II.3**
Empirical formula	$C_{36}H_{43}ClCoN_5O_2P_2S_2$
Formula weight	798.19
Temperature/K	293(2)
Crystal system	monoclinic
Space group	C2
a/Å	20.013(7)
b/Å	10.3796(17)
c/Å	22.946(7)
α/°	90
β/°	121.57(4)

γ/°	90
Volume/Å^3	4061(3)
Z	4
ρ_{calc}g/cm^3	1.306
μ/mm^{-1}	0.707
F(000)	1664
Radiation	MoKα (λ = 0.71073)
2Θ range for data collection/°	4.092 to 41.632
Index ranges	-20 ≤ h ≤ 15, -10 ≤ k ≤ 7, -16 ≤ l ≤ 22
Reflections collected	4901
Independent reflections	3290 [R_{int} = 0.1302, R_{sigma} = 0.2029]
Data/restraints/parameters	3290/1/454
Goodness-of-fit on F^2	1.362
Final R indexes [I>=2σ (I)]	R_1 = 0.1856, wR_2 = 0.4229
Final R indexes [all data]	R_1 = 0.2389, wR_2 = 0.4713

Preparation of [Co(EtSNS)I(DMF)$_2$] (II.4). 0.1 mmol of metal precursor CoI_2 (31.27 mg) were dissolved with 0.1 mmol of HEtSNS (56.00 mg) in 5 ml of DMF. It was then added NEt_3 dropwise, waiting 5' between drops, until the solution clouded. The percipitate was centrifuged and the mother liquor allowed to slowly evaporate in a dry environment. This afforded small crystals suitable for X-ray diffraction. (Yield 27%)

Compound	**II.4**
Empirical formula	$C_{36}H_{44}CoIN_5O_2P_2S_2$
Formula weight	186.02
Temperature/K	293(2)
Crystal system	monoclinic
Space group	Cc

a/Å	10.5557(15)
b/Å	19.965(3)
c/Å	19.612(3)
α/°	90
β/°	95.175(12)
γ/°	90
Volume/$Å^3$	4116.4(9)
Z	4
$\rho_{calc}g/cm^3$	1.351
μ/mm^{-1}	0.389
F(000)	1749
Crystal size/mm^3	0.3 × 0.2 × 0.1
Radiation	MoKα (λ = 0.71073)
2Θ range for data collection/°	4.08 to 41.608
Index ranges	$-10 \leq h \leq 10$, $-19 \leq k \leq 19$, $-19 \leq l \leq 19$
Reflections collected	12963
Independent reflections	4300 [R_{int} = 0.1642, R_{sigma} = 0.1655]
Data/restraints/parameters	4300/2/448
Goodness-of-fit on F^2	1.259
Final R indexes [I>=2σ (I)]	R_1 = 0.1410, wR_2 = 0.3425

Preparation of [Co(EtSNS)(NO_3)(H_2O)]·2DMF (II.5). $Co(NO_3)_2 \cdot 6H_2O$ (58.20 mg, 0.2 mmol) was dissolved in 5 ml DMF with 0.1 mmol of HEtSNS (56.00 mg). To the solution under stirring was added NEt_3 dropwise, waiting 5' between drops, until the solution clouded. The percipitate was centrifuged and discarded. The mother soluton was placed at 4°C and after 24 hours purple cristals suitable for X-ray diffraction formed on the walls of the vial. (Yeld 68%)

Compound	**II.5**
Empirical formula	$C_{36}H_{46}CoN_6O_6P_2S_2$
Formula weight	843.78
Temperature/K	185(2)
Crystal system	monoclinic
Space group	Pn
a/Å	10.8015(2)
b/Å	10.4785(2)
c/Å	18.1410(4)
α/°	90
β/°	95.543(2)
γ/°	90
Volume/Å^3	2043.66(8)
Z	2
ρ_{calc}g/cm^3	1.371
μ/mm^{-1}	0.651
F(000)	882
Crystal size/mm^3	0.5 × 0.5 × 0.3
Radiation	Mo Kα (λ = 0.71073)
2Θ range for data collection/°	3.886 to 56.564
Index ranges	$-14 \leq h \leq 14$, $-13 \leq k \leq 13$, $-24 \leq l \leq 24$
Reflections collected	26084
Independent reflections	10132 [R_{int} = 0.0336, R_{sigma} = 0.0343]
Data/restraints/parameters	10132/76/504
Goodness-of-fit on F^2	1.028
Final R indexes [I>=2σ (I)]	R_1 = 0.0395, wR_2 = 0.0965
Final R indexes [all data]	R_1 = 0.0429, wR_2 = 0.0987

Preparation of [Co(EtSNS)(EtSNP)(EtNC)]PF_6 (II.6). Complex **II.1** (65.30 mg, 0.05 mmol), HEtSNS) (58.17 mg, 0.1 mmol) and 0.75 ml of NEt_3 were dissolved in 5 ml of acetone. 0.2 mmol of KPF_6 were added to the mixture, that was left under stirring overnight. The white precipitate that formed was

centrifuged and the mother solution was layered with exane and placed at 4° C. After three days small red cubical crystals formed on the walls of the vial. These were collected and washed with a 1:2 mixture of hexane and DCM, then recrystallized in DCM layered with hexane to obtain X-ray diffrction sutable crystals. (Yield 42%)

Compound	**II.6** · 1/3CH2Cl2
Empirical formula	$C_{60.3}H_{60.7}Cl_{0.7}Co_1F_6N_6P5S_3$
Formula weight	2633.39
Temperature/K	100
Crystal system	triclinic
Space group	P-1
a/Å	12.088(2)
b/Å	13.826(3)
c/Å	19.228(4)
α/°	77.67(3)
β/°	80.87(3)
γ/°	80.76(3)
Volume/Å^3	3072.7(12)
Z	2
ρ_{calc}g/cm^3	1.423
μ/mm^{-1}	0.602
F(000)	1359
Crystal size/mm^3	0.03 × 0.03 × 0.02
Radiation	synchrotron (λ = 0.700)
2Θ range for data collection/°	2.154 to 57.298
Index ranges	-16 ≤ h ≤ 16, -18 ≤ k ≤ 18, -25 ≤ l ≤ 26
Reflections collected	104314
Independent reflections	16330 [R_{int} = 0.0378, R_{sigma} = 0.0215]
Data/restraints/parameters	16330/160/827
Goodness-of-fit on F^2	1.054
Final R indexes [I>=2σ (I)]	R_1 = 0.0372, wR_2 = 0.1035

Final R indexes [all data]	$R_1 = 0.0420$, $wR_2 = 0.1075$

Preparation of II.7. A solution composed of 10 ml of dry DCM, in which we dissolved 0.1 mmol of **II.1** (130.61 mg), was placed in a Schlenk with a capacity of 30 ml (internal diameter of 1.5 cm) fitted with a rubber seal. To this solution was firstly added 2 ml of dry DCM containing 0.2 mmol of $NaBH_4$. After establishing that no reaction was occurring, we added 0.5 ml of dry methanol, maintaining the solution under a vigorous stirring. Immediately the emeraldine solution started to turn brown and to evolve gas. After five minutes we ventilated the Schlenk and noticed that the solution was noticeably hot. After one hour the evolution of gas and heat was over. We stopped the stirring and let the reaction to cool down to room temperature. After two hours the solution appeared of a reddish brown and slightly foggy, while a whiteish powder settled to the bottom. We layered hexane directly in the Schlenk and placed the vessel at 4° C in order to slow the diffusion rate of the antisolvent. After two days small irregular crystals of a brownish violet appeared on the walls of the vessel. The crystals proved unstable upon exposure to air and moisture.

Preparation of [Ni(EtSNS)(NO_3)(H_2O)]·2DMF (II.8a). $Ni(NO_3)_2 \cdot 7H_2O$ (29.08 mg, 0.1 mmol) was dissolved in 5 ml DMF with 0.1 mmol of HEtSNS (56.00 mg). To the solution was added 0.075 mL of NEt_3 and the reaction was

stirred for 1 hour. The mother soluton was left to solwly evaporate and after 15 days green crystals started to form. To obtain crystals suitable for X-Ray diffraction it occourred a month of very slow evaporation. (Yeld 87%)

Compound	**II.8a**
Empirical formula	$C_{36}H_{44}N_6NiO_6P_2S_2$
Formula weight	178.96
Temperature/K	293(2)
Crystal system	orthorhombic
Space group	$Pna2_1$
a/Å	20.2249(9)
b/Å	10.5133(4)
c/Å	19.4026(8)
α/°	90
β/°	90
γ/°	90
Volume/Å^3	4125.6(3)
Z	4
ρ_{calc}g/cm^3	1.297
μ/mm^{-1}	0.214
F(000)	1697
Crystal size/mm^3	0.45 × 0.3 × 0.25
Radiation	MoKα (λ = 0.71073)
2Θ range for data collection/°	4.028 to 46.512
Index ranges	$-22 \leq h \leq 22$, $-11 \leq k \leq 11$, $-21 \leq l \leq 21$
Reflections collected	35787
Independent reflections	5932 [R_{int} = 0.0888, R_{sigma} = 0.0447]
Data/restraints/parameters	5932/1/512
Goodness-of-fit on F^2	1.054
Final R indexes [I>=2σ (I)]	R_1 = 0.0619, wR_2 = 0.1545
Final R indexes [all data]	R_1 = 0.0718, wR_2 = 0.1639

Preparation of [Ni(EtSNS)(NO_3)(DMF)] (II.8b). The preparation of this compound is the same of compound 8, but we used dry DMF and the evaporation of the solvent took place in a dry environment. (Yield 90%)

Compound	**II.8b**
Empirical formula	$C_{33}H_{36}N_5NiO_4P_2S_2$
Formula weight	749.44
Temperature/K	293(2)
Crystal system	triclinic
Space group	P-1
a/Å	11.1270(6)
b/Å	11.2191(4)
c/Å	14.7335(7)
α/°	81.702(3)
β/°	89.673(4)
γ/°	71.238(4)
Volume/Å^3	1721.66(14)
Z	2
ρ_{calc}g/cm^3	1.446
μ/mm^{-1}	0.812
F(000)	780
Crystal size/mm^3	? × ? × ?
Radiation	synchrotron (λ = 0.700)
2Θ range for data collection/°	3.812 to 55.632
Index ranges	$-14 \leq h \leq 14$, $-14 \leq k \leq 14$, $-19 \leq l \leq 19$
Reflections collected	25098
Independent reflections	7938 [R_{int} = 0.0376, R_{sigma} = 0.0298]
Data/restraints/parameters	7938/0/428
Goodness-of-fit on F^2	1.159
Final R indexes [I>=2σ (I)]	R_1 = 0.0353, wR_2 = 0.1032
Final R indexes [all data]	R_1 = 0.0361, wR_2 = 0.1074

Preparation of [Ni(EtSNS)(CH_3COO)(DMF)] (II.8c). The preparation 8b was carried out using the same procedure used in the sinthesis of compound 8, but 0.1 mmol (24.88 mg) of $Ni(CH_3COO)_2$ was used instead of the nickel nitrate. (Yield 74%)

Compound	**II.8c**
Empirical formula	$C_{35}H_{40}N_4NiO_3P_2S_2$
Formula weight	749.48
Temperature/K	293(2)
Crystal system	monoclinic
Space group	$P2_1/c$
a/Å	11.4068(3)
b/Å	18.5185(4)
c/Å	17.5666(5)
α/°	90
β/°	105.033(3)
γ/°	90
Volume/$Å^3$	3583.72(17)
Z	4
$\rho_{calc}g/cm^3$	1.389
μ/mm^{-1}	0.788
F(000)	1568
Crystal size/mm^3	? × ? × ?
Radiation	MoKα (λ = 0.71073)
2Θ range for data collection/°	3.256 to 56.564
Index ranges	$-15 \leq h \leq 15$, $-24 \leq k \leq 24$, $-23 \leq l \leq 2$
Reflections collected	41324
Independent reflections	8889 [R_{int} = 0.0500, R_{sigma} = 0.0344]
Data/restraints/parameters	8889/0/457
Goodness-of-fit on F^2	1.044
Final R indexes [I>=2σ (I)]	R_1 = 0.0406, wR_2 = 0.0896
Final R indexes [all data]	R_1 = 0.0581, wR_2 = 0.0984

BIBLIOGRAPHY

[1] a) P. Gandeepan, C. H. Cheng, *Acc. Chem. Res*., **2015**, 48 *(4)*, 1194-1206. b) X. B. Lu, D. J. Darensbourg, *Chem. Soc. Rev.*, **2012**, 41, 1462–1484. c) S. St John-Campbell, J. A. Bull, *Adv. Synth. Catal.* **2019**, *361*, 3662.

[2] a) L. M. Gilby, B. Piggott, *Polyhedron*, **1999**, 18 *(7)*,1077-1082. b) M. C. Aragoni, M. Arca, A. Garau, F. Isaia, V. Lippolis, G. L. Abbati, A. C. Fabretti, *Z. anorg. allg. Chem*., **2000**, 626, 1454-1459.

[3] a) D. L. Cronin, J. R. Wilkinson, L. J. Todd, *Journal of Magnetic Resonance*, **1975**, 17 *(3)*, 353-361. b) C. C. Mokhtarzadeh, A. E. Carpenter, D. P. Spence, M. Melaimi, D. W. Agnew, N. Weidemann, C. E. Moore, A. L. Rheingold, J. S. Figueroa *Organomet.*, **2017**, 36 *(11)*, 2126-2140.

[4] a) E. Simo´n-Manso, M. Valderrama, D. Boys, *Inorg. Chem.* **2001**, 40 *(14)*, 3647-3649. b) R. Rösler, C. Silverstru, G. Espinosa-Pérez, I. Haiduc, R. Cea-Olivares, *Inorganica Chim. Acta*, **1996**, 241 *(2)*, 47-54. c) P. Bhattacharyya, J. Novosad, J. Phillips, A. M. Slawin, D. J. Williams, J. D. Woollins, *J. Chem. Soc., Dalton Trans.*, **1995**, 1607-1613

Chapter 3: Loading of a Molecular Thermometer for Accurate Intracellular Thermal Analysis

OBJECTIVES:

Preliminary screening:

- Find the best pore size
- Most suitable surface chemistry
- Most efficient loading chemistry

Preliminary characterization:

- Did the thermometer enter the pores? → IR
- Loading efficiency

Bulk synthesis of loaded Si nanoparticles

- For a more robust and thoroughly characterization
- For in-vitro studies of cellular uptake and thermal imaging

Characterization:

- TEM
- DLS
- Preliminary photoluminescence study

INTRODUCTION

The idea behind molecular thermometers is to be able to follow in real time the local temperature within a cell, instead of obtaining an average temperature reading. With a molecular thermometer, we could use temperature variations to follow the evolution of metabolic processes and monitor cell response to external stimuli such as stress and alien molecules, e.g. drugs. Over the last ten years, this topic has drawn a lot of attention, and we have seen the development of a wide variety of different approaches to obtain the same result. Six main strategies have been devised, that will be summarized in the following list.[1]

- Fluorescent polymeric thermometers. These molecular devices work as follows: they are small particles composed of copolymers characterized by a fluorescent subsystem and an auxiliary portion working as quencher. As a function of temperature, the interaction between the two subsystems varies, and as fluorescent intensity itself is strongly affected by the interactions, temperature variations are directly reflected into a modification of the fluorescence spectrum.
- Gold nanoclusters.
- Quantum dots.
- Nanodiamonds.
- Molecular thermometers, i.e. small molecules
- Small molecules capable of targeting specific regions of the cell.

All these approaches present one or more serious drawbacks when applied in cells. The main problem is related with the low sensitivity of the system to temperature variations, i.e. the fact that they cannot detect temperature variations below a certain threshold, and normal cellular processes involve temperature variations well below this threshold. The second main problem is quenching: in the presence of oxygen, the fluorescence is quenched. Thus, the presence of oxygen affects temperature readings to a significant extent; a possibility to cope with this is to work in anoxic conditions, which however puts the cell under stress. The extent of this stress is hard to determine and introduces a degree of uncertainty on temperature readings. A third serious problem is cellular uptake: even if the perfect, oxygen insensitive thermometer capable of detecting the smallest temperature variation was produced, still we would have the problem of incorporating it into the cell. Only few cell types are resistant enough to sustain an injection, and those who are undergo a significant stress in the procedure. Furthermore, even if the thermometer can be easily incorporated into the cell, nothing guarantees that they can be efficiently cyto-dispersed.

After these initial considerations have been laid out, we will proceed to present the structure and properties of our system. The thermally sensitive unit is $[Cu_5(EtSNS)_3](PF_6)_2$, a cluster of five Cu(I) ions held in place by three $EtSNS^-$

ligand molecules. This system has been shown to be an excellent molecular thermometer, owing to the temperature dependence of both its fluorescence intensity and lifetime. Noteworthily, thermometers designed to follow the variation of lifetimes are more accurate than those based on fluorescence intensities.[2]

Our system has a 0.01 K thermal resolution in a wide temperature range (from -70 to +70º C), and its fluorescence does not depend on the environment. Our thermometer alone is not water soluble, and thus cannot be cyto-dispersed, but by incorporating it into nanoparticles of porous Si, we can specifically target cellular uptake with drug delivery purposes and good bio-compatible and bio-degradable properties (Figure 3.1).[3]

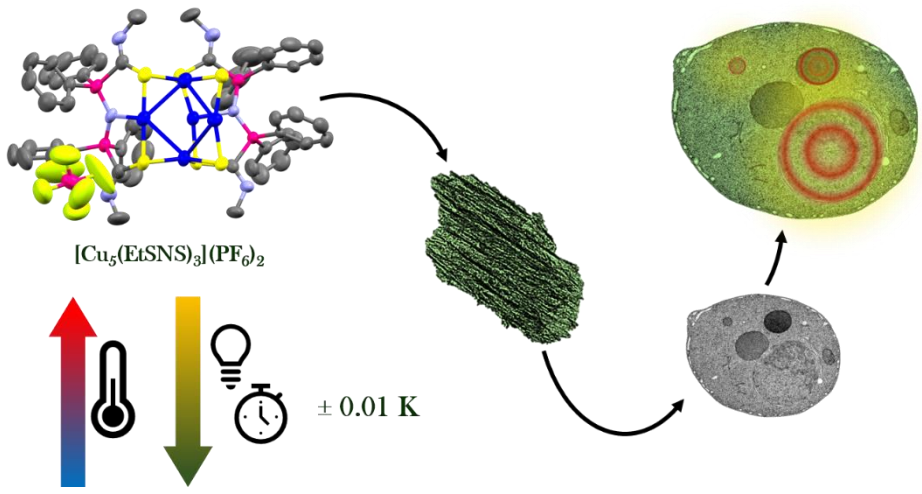

*Figure 3.1:*Graphical abstract

Porous silicon nanoparticles are synthetized in two steps: electrochemical etching of a p+ or p++ doped Si wafer with an HF solution under direct pulsate current with appropriate intensity and high-low current times achieve a thin porous film on the wafer exposed face, with the channels perpendicular to the (100) crystal plane. This thin film is then detached from the wafer with an higher intensity current (a sufficientrly high current potential do not achieve pores but electropolishing, a isotropic etching) and then sonicated. As the thin film presents pores with periodically finer walls (due to the pulsate current applied) the sonication will break preferentially the finer planes, achieving a fine control over the final dimensions of the particles. The porous silicon can be functionalized with a variety of techniques, from the deposition of a polymeric or carbonious layer to an oxide coating. The most interesting technique for this thesis is the functionalization of the surface with chemically bonded carbon chains that may be further functionalized with functional groups, for example ammines, carboxylic acids or phosphines.

In this way, we designed a system that acts in a twofold way: i) owing to the loading, we obtain nanoparticles able to detect temperature variations, and ii) the nanoparticles themselves can release the guest within the cell allowing a good dispersion in the cyto-environment. A further advantage of this dual system is the protection provided to the thermally active compound by the scaffold: the thermometer, indeed, is subject to slow degradation by chlorides. For this reason,

even if we found an alternative way of dispersing the thermometer in the cell, we would face its degradation, which in turn would affect temperature readings. When loaded into the nanoparticle, the thermometer is protected by this degradation, thus prolonging its lifetime.

RESULTS AND DISCUSSION

The first objective of the stay at UCSD was to load the molecular thermometer onto Si nanoparticles. Our first approach was to simply soak the freshly-etched thin film in an acetone solution of $[Cu_5(EtSNS)_3](PF_6)_2$. Unfortunately, during the etching process the surface of the pores develops hydroxyl groups, whose polarity discourages loading of the hydrophobic metal cluster. In order to solve this problem, we functionalized the surface of the thin film with a hydrophobic layer (see Experimental Section).[4] First, we soak the thin film, then we sonicate to obtain the loaded nanoparticles. This proved effective, as we were able to load the thermometer into the pores of this film to a satisfactory extent. However, not only did we strive to achieve this loading, but also to maximize the thermometer uptake. While this first loading proved to be feasible, we encountered two main problems, both related to the pore structure, which in turn depends on the etching current profile. This profile is characterized by a continuous direct low current with periodic high current spikes (see Experimental Section). Since pores are created from the surface down into the bulk, and the size of the pore is directly proportional to the intensity of the current and etching velocity, we obtain a regular alternation of section size within the pore; when the current is low, we have a small pore section, which increases during current spikes.

This regular alternation of the pores' size allows for preferential rupture planes, much like the perforated profile of a sheet of stamps. When force is applied, the

system will respond by breaking at predetermined points. The first problem is that owing to the pores' geometry, obtaining a complete loading of the thin film is challenging; this is probably due to the presence of microaggregates formed during the loading which obstruct the pores. Our thermometer is highly prone to aggregation and crystallization, which is an additional challenge, because microaggregates can be formed in the large-section regions of the pores, and by drifting into the narrow-section regions can block the loading preventing any further reactivity. The second problem is related with sonication, which can break pores on the larger sections, where Si walls are at the thinnest; this leads to the release of the thermometer that was hosted in the pore. This problem is accentuated by the fact that during sonication we have to use a dispersion medium wherein our thermometer is insoluble. In turn, this means that metal cluster released during sonication aggregates and deposits on the surface of the nanoparticles in an oily coating. To address this problem, we resorted to sonicate the functionalized thin film before loading, inverting the order of the processes of loading and sonication. In this way, we obtained clean nanoparticles with homogenous pores which are been loaded with the thermometer. This improved the loading percentage from 2 to 5%. However, also this second approach presented a serious limitation, i.e. the fact that while nanoparticles were coated in thermometer, and thus aggregated, they lost a significant amount of metal cluster when washed with a mixture of acetone and hexane, whose best

proportion yielded a loading of 5%. This is due to the chemical nature of the nanoparticle regions exposed at the rupture planes: these portions of the nanoparticles, being more polar as they were not functionalized, have a higher affinity for the washing solution than for the cluster, which partially reverses the loading process (Figure 3.2).

Actually, the presence of polar portion on the nanoparticles is desirable for *in vivo* application, since these regions should confer to the final system the capability of being dispersed in water. However, even with the 5% loading obtained with the previous strategy, the polarity is not enough to produce this

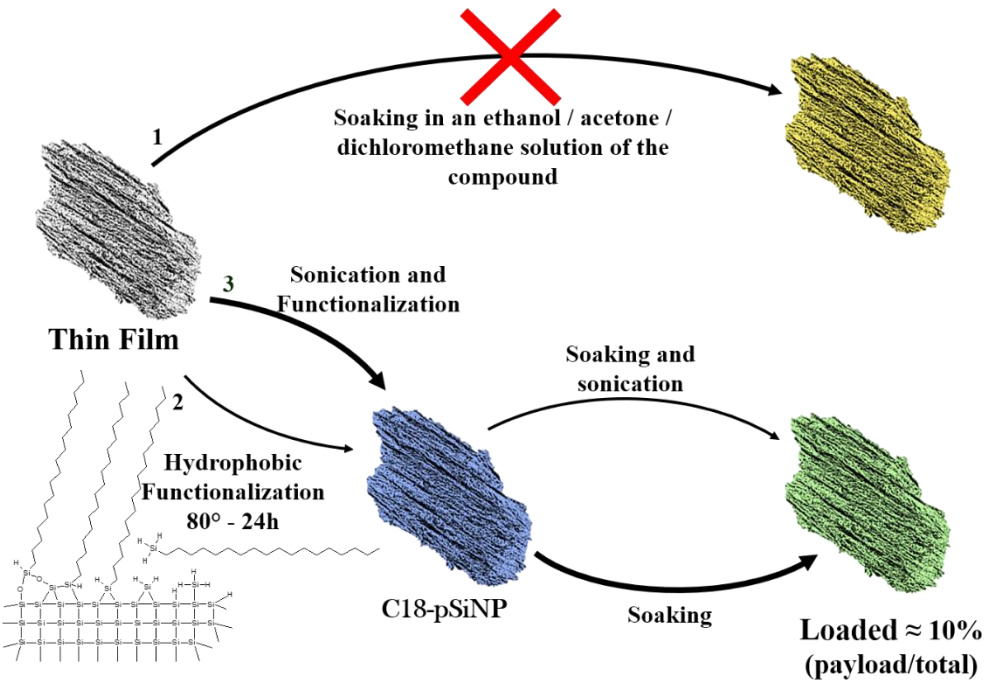

Figure 3.2: Visual recap of the three strategies of synthesis, functionalization and loading.

effect. For this reason, an alternative strategy has been devised. This third approach involves thin film sonication before functionalization. Ethanol was

used instead of water, as the former is a more efficient film disruptor, since water proved much more difficult remove completely from the pores. Water in the pores would not allow the functionalising agent to completely permeate, resulting in incomplete surface functionalization. With the same method (see Experimental Section) we functionalized the nanoparticles (C18-SiNP) gaining a first advantage. Indeed, functionalizing directly the nanoparticles rather than the thin film leads to a more homogenous coating. After washing the nanoparticles, a loading in acetone was performed with a subsequent washing away of the cluster in excess. In this step, a further advantage is gained: it becomes easier to understand if nanoparticles have a lower covering in cluster, since they will show a lower tendency to aggregate in hexane after washing. This method yielded a loading between 9 and 11% in the various attempts, with the certainty of having segregated all of the guest inside the pores (Figure 3.2). The loading was assessed by weighing dry C18-SiNP before and after the loading process. Inside these pores, the guest is better shielded from the environment than at the surface. However, a problem still remains, i.e. the fact that these nanoparticles cannot for sure be dispersed in water: While in the second approach we had polar regions on the nanoparticles, which were anyway insufficient to confer water

dispersibility to the nanoparticles, in this third case the polar regions are absent, yielding a material that cannot be dispersed in water. This loading methodology is peculiar because the loading is perfectly reversible: when immerse in acetone, the cluster leaks away from the nanoparticle without affecting the stability of either and the recovered nanoparticles can host a new guest (Graph 3.1). On these nanoparticles we performed a preliminary fluorescence characterization via time-gated imaging. Figure 3.3 shows the two images, one at time 0, showing the fluorescence of the cluster and of the SiNP, reading a peak at 2.5 x 10^5 counts, the second, taken after 5 μs, shows only the fluorescence of the SiNP, as the time

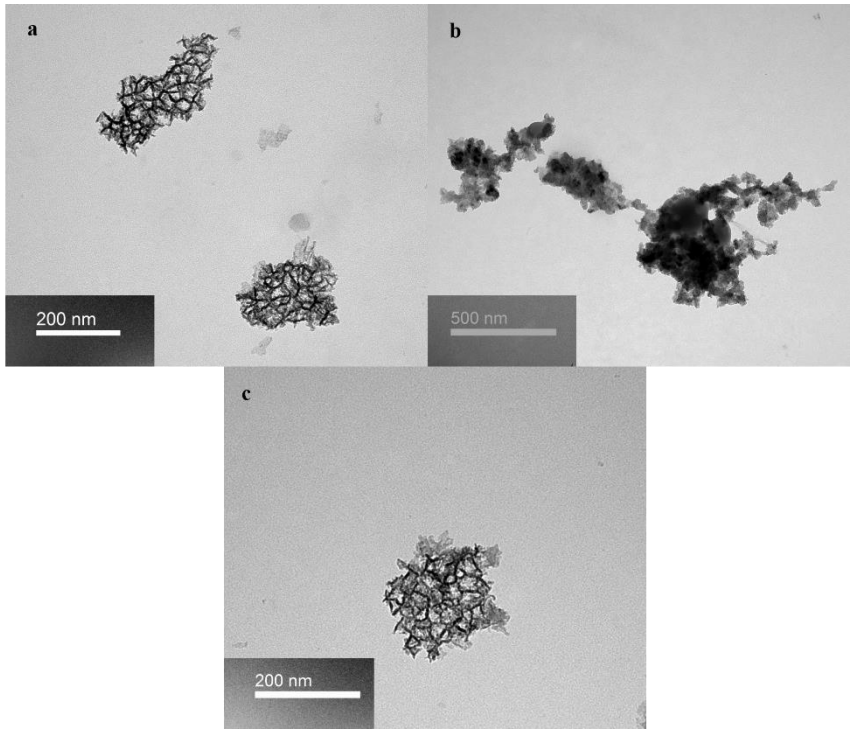

Figure 3.3: a- freshly sonicated C18-pSiNP; b- freshly sonicated C18-pSiNP from a loaded thin film (it is clearly appreciable an oily film that aggregate the nanoparticles); c- loaded C18-pSiNP

of decay of the cluster is much shorter at room temperature, and reads a peak at 4 x 10^5. This leads to the conclusion that, although both the cluster and the SiNP are fluorescent, the intensity of the cluster is 20 times higher than the one of the particles. This is confirmed by the fluorescence spectrum of the loaded nanoparticles (also reported in Figure 3.3) that shows a peak at 640 nm, assigned to the cluster, with a small shoulder at 840 assigned to the SiNP. This concludes the experimental work at UCSD.

Once back in Parma, we started researching into a coating that allows nanoparticles to be stabilized in aqueous medium. To do so, we developed a

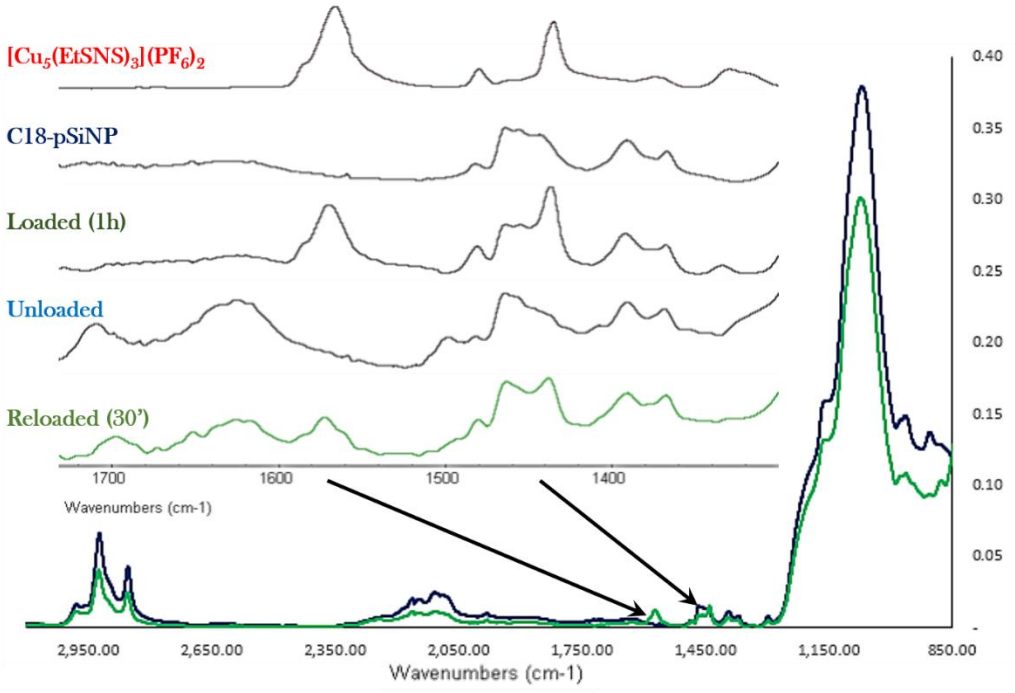

Graph 3.1: IR spectrum of various species that demonstrate the loading, unloading and reloading of the cluster.

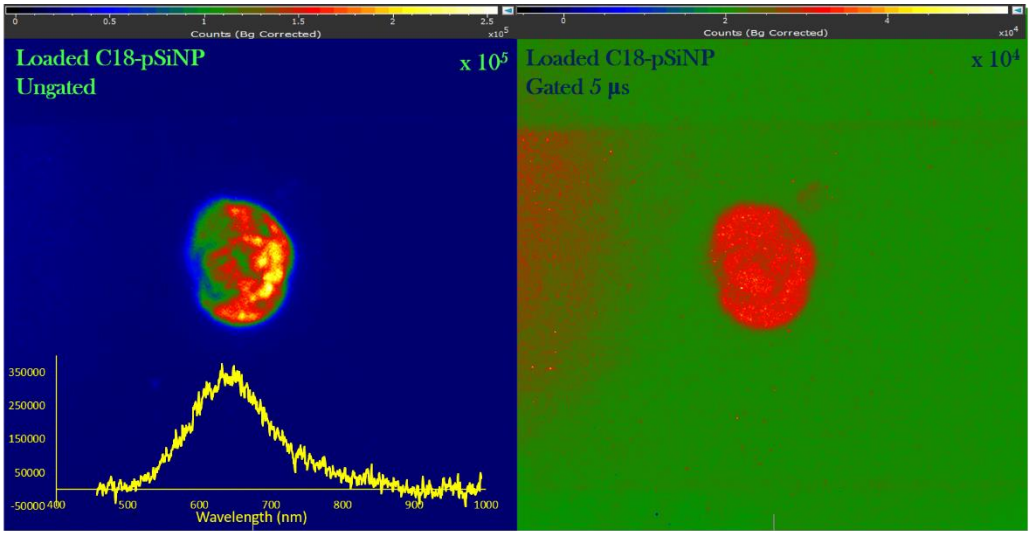

Figure 3.4: Time-gated imaging of the loaded C18-pSiNP and their emission spectrum.

procedure, that to the best of our knowledge is unprecedented, and yielded satisfactory results. We chose TWEEN-30 as dispersant because of its popularity in biological assays, which makes it compatible with *in vivo* conditions. The problems of a classical coating are the following: TWEEN-30 surfactant is not miscible with hexane, which is the dispersant of the nanoparticles, so we cannot perform a direct coating. Furthermore, its viscosity is extremely high, so that its direct use with dry nanoparticles is a painfully slow and not particularly efficient process. Since our nanoparticle are not dispersible in water, a mixture of TWEEN-30 and water is not an option, as it would result in the coating of aggregates and not isolated nanoparticles.

We proceeded as follows: in a plastic vessel, chosen because TWEEN-30 does not wet the container's surf, we used an Eppendorf. Shaking, we obtained a 5:1

emulsion of TWEEN-30 in the hexane where the nanoparticles are dissolved. This emulsion was sonicated within the closed vessel for 1 h in order to start transferring the nanoparticles form hexane to TWEEN-30. Later, the container was opened and sonication was continued for another hour after complete evaporation of the hexane. At this point, water was added with a further 30 min of sonication, after which the system was left to equilibrate until all aggregates precipitated. The remaining solution of nanoparticles dispersed water-TWEEN-30 was centrifugated and the precipitate washed with water to eliminate TWEEN-30 in excess. The nanoparticles were then dispersed in a 1% solution of TWEEN-30 in water. In Graph 3.2 is reported the comparison between the DLS spectrum of freshly etched SiNP and TWEEN-30 coated C18-pSiNP, that shows a slight enlargement of the particles hydrodynamic radius and their good dispersion in water.

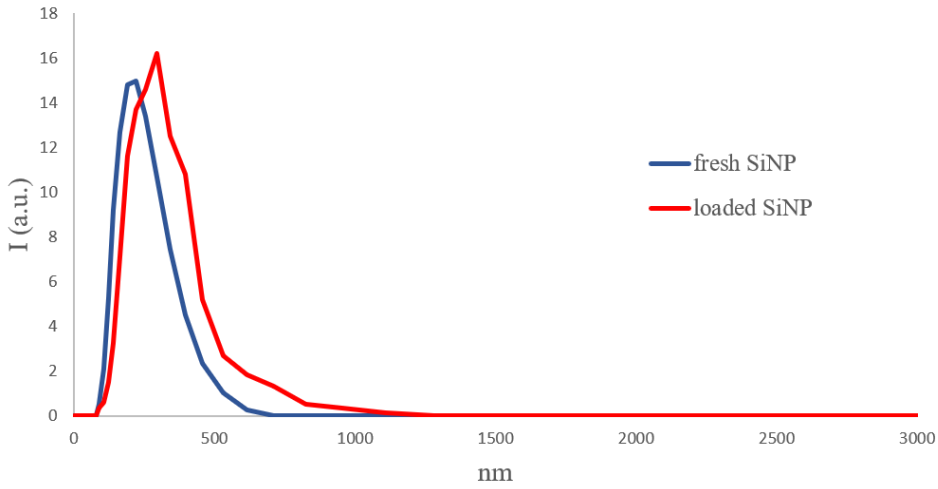

Graph 3.2: DLS spectra of freshly etched SiNP and TWEEN-30 coated C18-pSiNP.

CONCLUSIONS

We have managed to address all the objectives of the project presented in this Chapter, both during the stay at UCSD and back at the University of Parma. We obtained a system that incorporates our fluorescent molecular thermometer into the nanopores of our silica nanoparticles. Further work will include a more detailed characterization of the luminescence of our loaded nanoparticles and *in vivo* testing for biomedical applications.

EXPERIMENTAL SECTION

1- Silicon etching:

A chip-grade p-doped silicon wafer was etched with direct current modulated with a Brag-stack function (300 cycles of 402mA for 1.818s and 3216mA for 0.363s) in order to obtain a nano-porous silicon thin film with a periodic perforation running perpendicular to the pores. This approach leads to a post-stamp like periodic weakness in the thin film that permits a quick and easy disaggregation to homogeneously sized porous nanoparticles.

2- Ultrasonic disaggregation:

The thin film was washed three times in absolute ethanol and then submerged in the same solvent in a 20 ml glass vial. The vial was then placed in an ultrasonic bath for 24 to 36 hours to break apart the silicon film into suitable sized nano particles.

3- Hydrophobic functionalization:

The broke-down thin film was dried and placed in a vial with 750ml of octadecylsilane, warmed up to 40° C . The vial was then sonicated briefly to ensure full pore penetration end then heated to 80° for 24 hours. To ensure that all the silane was removed at the end of the functionalization, the reaction mixture was sonicated for five minutes and then centrifuged at 40° C for 30

minutes at 12000 rpm with warm hexane. This washing step was repeated until the washing solvent did not left a white residue when dried. The particles were then suspended in hexane and centrifuged at 12000 rpm for two minutes, in order to discard all the material that was not fully broke into nanoparticles in the previous step. The brown-coloured supernatant is then stored in a tightly sealed glass vial.

4- Loading:

The nanoparticles were dried in vacuum and 5 mg were dispersed via sonication 5ml of acetone. 0.001 mmol of $[Cu_5(EtSNS)_3](PF_6)_2$ (22.83 mg) was dissolved in two ml of acetone and added to the vial. The mixture was then sonicated for 1 hour and left to homogenise for 3 hours. The nanoparticles were then separated via centrifugation and washed three times with a 1:1 mixture of acetone/hexane and then dispersed in pure hexane. The loading solution and the washes were then dried and the remaining $[Cu_5(EtSNS)_3](PF_6)_2$ weighted to gravimetrically establish the loading efficiency.

5- Coating:

Approximately 0.5 milligrams of loaded nanoparticles were sonicated in 5 ml of hexane for five minutes to ensure a good dispersion and then 1 ml of TWEEN-30 was added to the vial. The vessel was thoroughly shaken to

emulsify the two immiscible liquids and then left open while sonicated at room temperature, until all the hexane was evaporated. The gooey dispersion was then fluidified with 5 ml of distilled water and then centrifuged (30 minutes at 12000 rpm) and washed three times with distilled water. The particles were then suspended in 5 ml of a 100:1 mixture of water and TWEEN-30.

BIBLIOGRAPHY

[1] a) M. Nakano, T. Nagai *J. Photochem. Photobiol*., **2017**, *30*, 2-9. b) S. Uchiyama, et al. *Angew. Chem. Int. Ed.*, **2018**, *130*, 1-6.

[2] D. Cauzzi, R. Pattacini, M. Delferro, F. Dini, C. Di Natale, R. Paolesse, S. Bonacchi, M. Montalti, N. Zaccheroni, M. Calvaresi, F. Zerbetto, L. Prodi, Angew. Chem. Int. Ed., 2012, 51, 9662 –9665.

[3] a) V. S. Y. Lin, K. Motesharei, K. P. S. Dancil, M. J. Sailor, M. R. Ghadiri, *Science, **1997***, 278, 840-843. b) J. H. Park, L. Gu, G. Von Maltzahn, E. Ruoslahti, S. N. Bhatia, M. J. Sailor, *Nature Mat.,***2009**, 8 (4), 331. c) E. J. Anglin, L. Cheng, W. R. Freeman, M. J. Sailor, *Adv. Drug Deliv. Rev*., **2008**, 60 (11), 1266-1277. d) Michael J Sailor, *Porous silicon in practice: preparation, characterization and applications, **2009***, John Wiley & Sons.

[4] D. Kim, J. Joo, Y. Pan, A. Boarino, Y. W. Jun, K. H. Ahn, B. Arkles, M. J. Sailor, *Angew. Chem. Int. Ed.* **2016**, *55*, 6423.